The Abdus Salam
International Centre for Theoretical Physics

United Nations
Educational, Scientific
and Cultural Organization

International Atomic
Energy Agency

SMR 1673/50

AUTUMN COLLEGE ON PLASMA PHYSICS

5 - 30 September 2005

A Laboratory Experiment of a Cyclotron Maser Instability with Applications to Space & Laboratory Plasmas

presented by

R. Bingham

Rutherford Appleton Laboratory
Space Science & Technology Department
Didcot, U.K.

IPELS05 – 8th International Workshop on the Interrelationship between Plasma Experiments in Laboratory and Space – July 4th-8th, 2005, Tromsø, Norway

CCLRC

A Laboratory Experiment of a Cyclotron Maser Instability with Applications to Space & Laboratory Plasmas

Robert Bingham, **Barry J. Kellett**
Rutherford Appleton Laboratory
Space Science and Technology Department

Alan Cairns, Irena Vorgul
School of Mathematics & Statistics
University of St Andrews

Alan Phelps, Kevin Ronald, David Speirs, A.W. Cross, C.G. Whyte and C. Robertson
Department of Physics
University of Strathclyde

CCLRC Rutherford Appleton Laboratory

Motivation

Cyclotron Maser Radiation in Astrophysics, Space and Laboratory Plasmas

- Explain non-thermal cyclotron radio emission from stellar and planetary systems.
- Devise laboratory experiments to test the models.
- Laboratory experiment – "Table Top Aurora"
- Develop new methods for generating microwave maser radiation in the laboratory

CCLRC Rutherford Appleton Laboratory

Cyclotron Maser Emission

- Gyromagnetic Resonance

$$\omega - n\Omega - k_{||}v_{||} = 0$$

- $n = 0$ 1-D Cerenkov Condition
- $n \neq 0 \quad \omega \approx n\Omega \gg k_{||}v_{||}$ Cyclotron emission or absorption of O mode and X mode radiation.

Gyromagnetic Emission:

Cyclotron: non-relativistic

Gyrosynchrotron: mildly relativistic

Synchrotron: ultra relativistic

Cyclotron Instabilities

- Cyclotron instabilities are classified as **Reactive** or **Kinetic**
- **REACTIVE**
  - Due to particle bunching
  - Axial bunching – along z
  - Azimuthally bunching – bunching in angle ϕ associated with gyration in magnetic fields:-
    - Example Gyrotron
- **KINETIC** – Maser emission results from

$$k_{\parallel} \frac{\partial f}{\partial p_{\parallel}} > 0 \quad \text{or} \quad \frac{n\Omega}{v_{\perp}} \frac{\partial f}{\partial p_{\perp}} > 0$$

Parallel drive (left) Perpendicular drive (right)

- First discussion of electron cyclotron maser radiation was by Twiss (1958) to describe radio astronomical sources.
- Electron cyclotron maser emission is important for bright radio sources, from planets to the Sun to active flare stars.

History/Background

- X-ray and radio observations of "active" stars over the past 25 years have revealed a variety of different phenomena. Probably the most significant result is the important role played by magnetic fields in these stars (and the Sun!).
- However, many of the different observations appear contradictory when compared with each other.
- For example, the X-ray spectral data reveals ***thermal*** emission (in the 1-30 million K range), whereas the radio data is most often believed to be ***non-thermal*** and can have brightness temperatures in excess of 1000 million K!
- We started by reviewing the X-ray and radio observations of a wide range of active stars and collected together a number of observational "problems".
- We then proposed a particular magnetic configuration for these active stars and showed that with this one "assumption" we are able to explain all the observations…
- … and without any of the contradictions noted above!

Observational "Photofit"

- Two Temperature X-ray Plasma
  - 1-3 million K (i.e. very similar to the Sun!)
  - 10-30 million K & larger volume (much larger than the star, in fact – from eclipsing binaries)
- X-ray vs Radio Luminosity
- Polarized Radio Flares
- "Slingshot" Stellar Prominences
- First Resolved Radio Image - UV Ceti
- [X-ray Plasma Abundances]

X-ray vs Radio Luminosity of the Sun and Stars

- A remarkable correlation seems to apply to the radio and X-ray emission from solar flares and active stars – covering 8-10 orders of magnitude!
- But why should the X-ray and radio fluxes correlate at all?

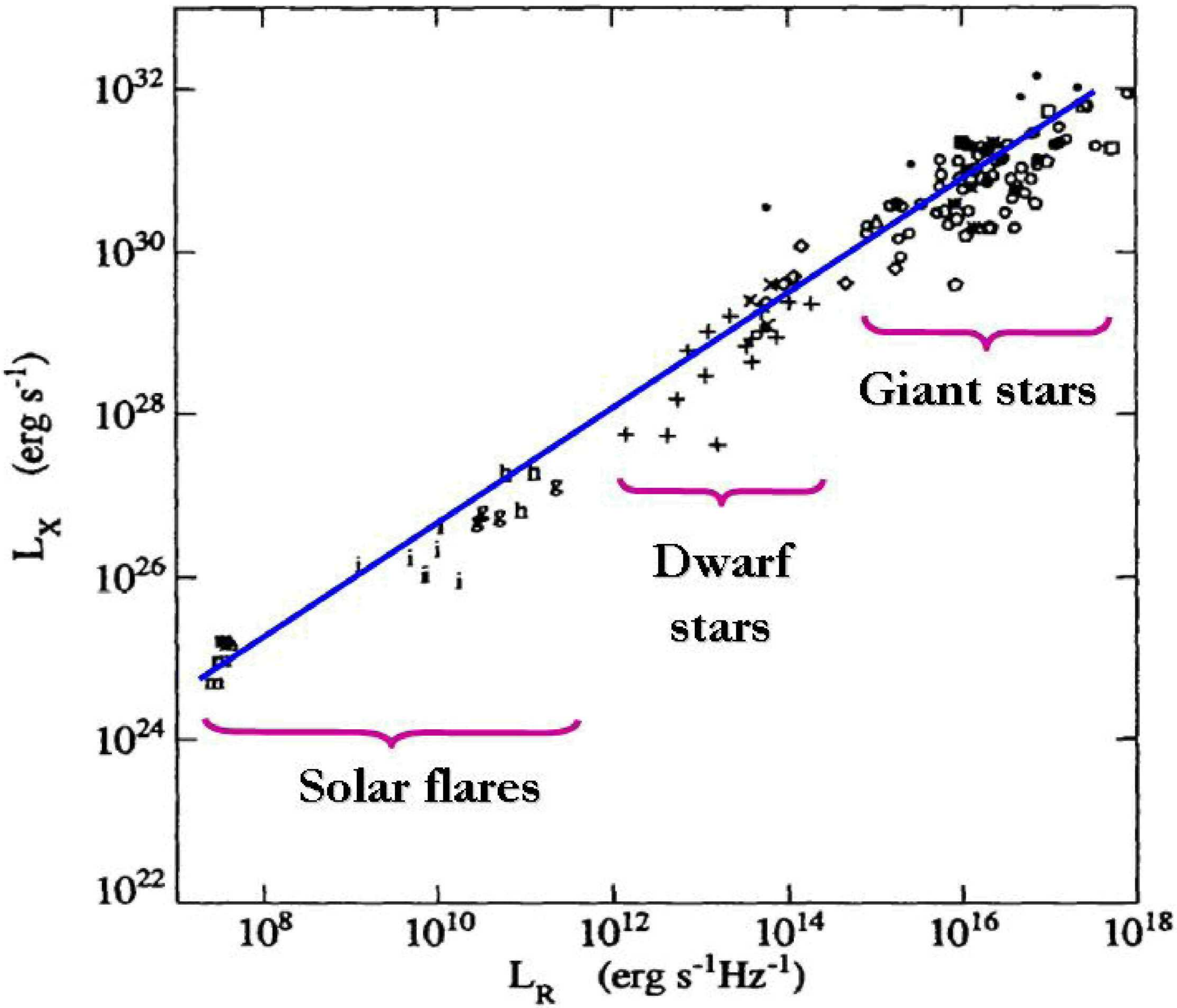

Polarized Radio Flares

Table 1. Radio flare on UV Ceti and YZ CMi.

Date (y/m/d)	Time (UT)	I_{Peak} (mJy)	Circ.Pol.? (Y/N)	%CP	Left/Right	Radio λ (cm)	Ref.	Comments
UV Cet = L726-8AB								
1983/8/12		3.01 ± 0.15	Y	64.5 ± 10	R	20	KS85	A comp. (daily mean)
1983/8/13		2.17 ± 0.15	Y	64.5 ± 10	R	20	KS85	A comp. (daily mean)
1985/2/6	22:54	12	Y	42 ± 3	R	20	KJWM87	B comp.
	21:48		Y	100		20	KJWM87	A comp.
1985/3/22	19:37	4.00 ± 0.16	Y	100 ± 6	R	6	JKW89	A comp.
	20:19	6.5 ± 0.2	Y	57 ± 4	R	20	JKW89	A comp.
	20:55	11.9 ± 0.4	Y	72 ± 3	R	20	JKW89	A comp.
1985/8/4	11:40	10	Y	~60	R	20	KPWJ88	B comp.
	12:35	35	Y	~60	R	20	KPWJ88	A comp.
1986/6/28	15:36	217	Y	100	L	20	BB87	B comp. (radio spike, 120 s)
	16:33	80	Y	70	R	20	BB87	B comp.
	16:38	100	Y	70	R	20	BB87	B comp.
1994/01/06		~1	Y	<50	R	3.6	BGS96	B comp. (18 weak flares)
1991/01/06		~1	Y	100	R	6	BGS96	B comp.
1991/12/31	18:30	250	Y	100	L	20	SFKHBS95	B comp. (radio spike, 250 s)
1996/2/6	00:00	3×10	Y	~100	R	3.6	BCG98	A comp.
	01:50	33	Y	~100	R	3.6	BCG98	A comp.
YZ CMi								
		9.2	Y	94	L	20	KS88†	
1983/2/3		~5.5	Y?		R?	6	vdO96	Slight RCP excess?
1983/10/25	08:37	~5	Y?	10	L	6	PWL85	Impulsive burst < 30 s; LCP *reduced* 50→10 per cent?
1984/12/10	07:30	30	Y	80	L	20	LW86	
1985/3/22	02:40	3.9	Y	80	L	20	JKW89	
1985/11/19	09:24	1.8	N	0		6	KPWJ88	
	10:00	14	Y	100	L	20	KPWJ88	
1986/6/23	20:00	15	N	<15		20	WLF88	
	20:10	~7	Y	~100	L	6	WLF88	After 20 cm event
1987/1/6	08:10	16	Y	~100	L	20	LW88	Total of 6 flares all 100 per cent LCP
1987/11/5	09:48	1600	Y	100	L	70	BBDD90	6.5 s burst
1988/10/6		42				6	SDZN93	

Stellar "sling-shot" Prominence

- **Slingshot prominences are seen in the optical spectra of stars as a dark "shadow" crossing the bright absorption lines of the star.**
- **The gradient of the shadow gives information about the relative velocity of the "cloud" and hence its position or height above the star.**

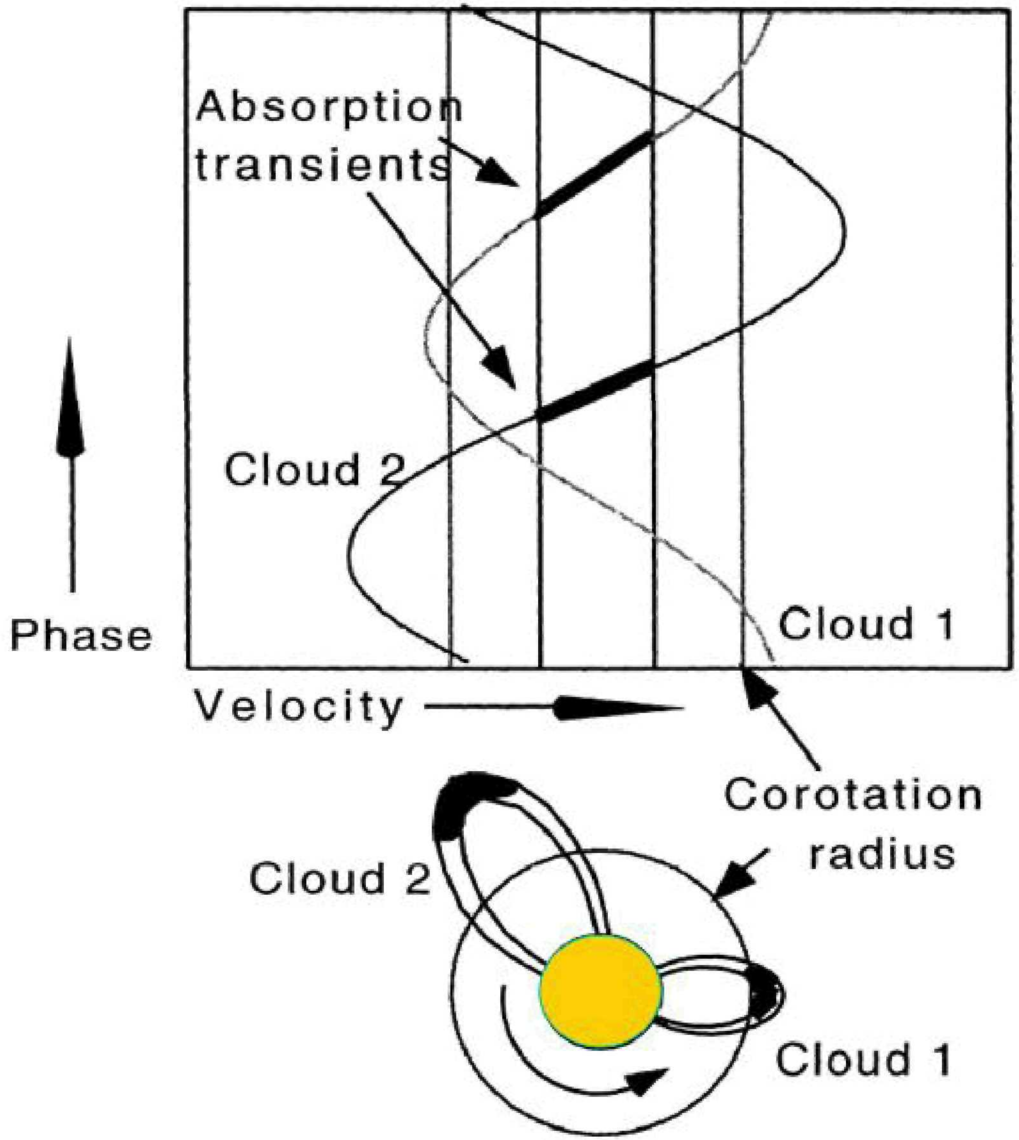

Figure 2. Schematic illustration of the relationship between the drift rate of an absorption transient and the distance of the cloud from the stellar rotation axis.

CCLRC Rutherford Appleton Laboratory

First Radio Image of a Star – UV Ceti

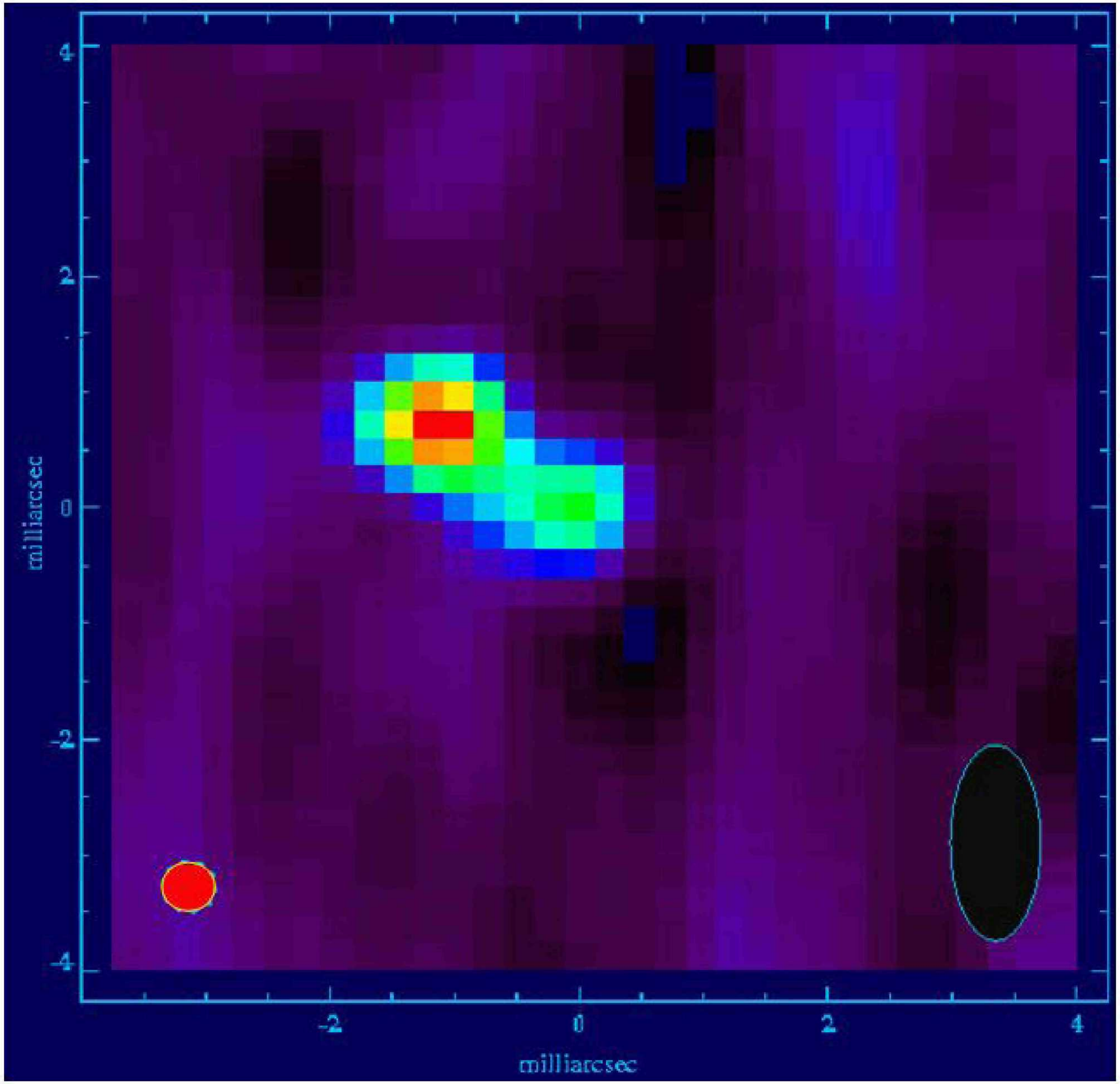

Laboratory Analog – a Toroidal Dipole Magnetic Trap

- A dipole magnetic field forms a natural magnetic trap and is responsible for the radiation belts around the Earth and other planets (*e.g.* Jupiter).
- It has been proposed as an ideal trap for fusion plasmas.
- The main feature of a dipole magnetic trap is the field strength minimum at the equator and increasing in strength towards the poles.
- In such a magnetic configuration charged particles will bounce back and forth between their mirror points in the northern and southern hemispheres.

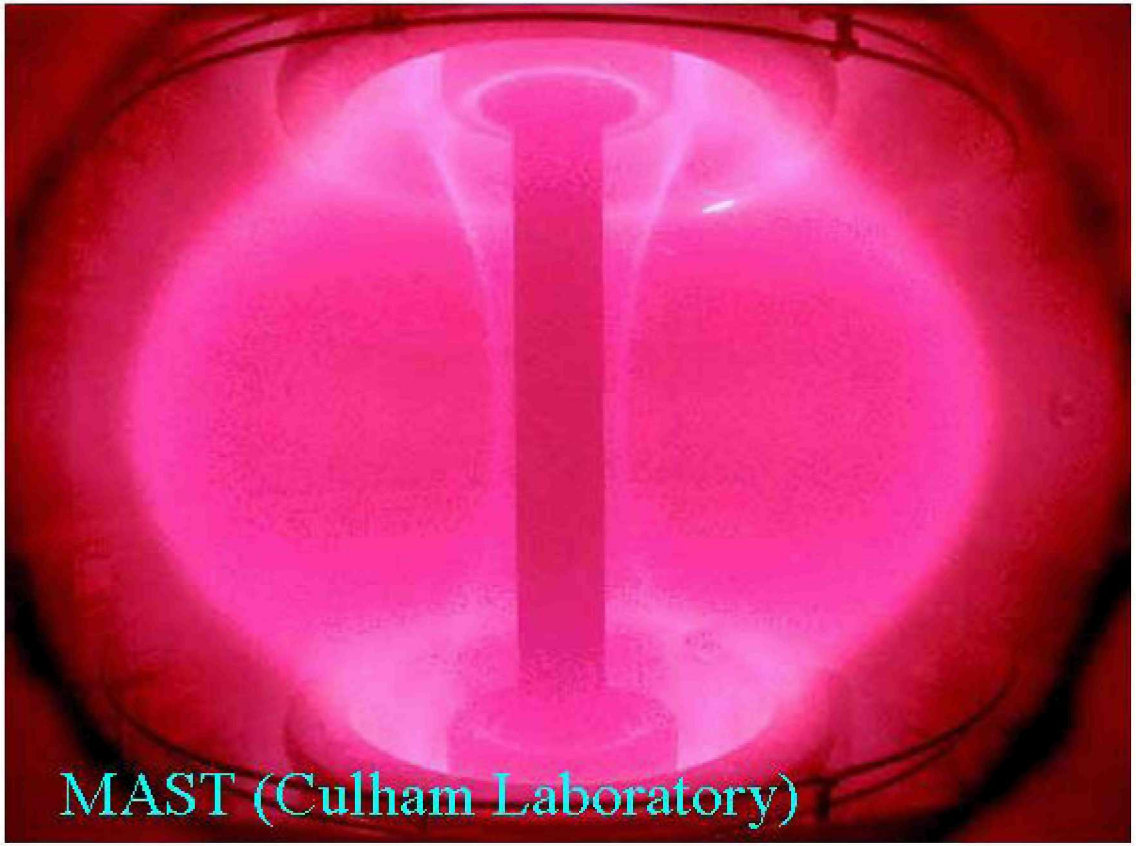

MAST (Culham Laboratory)

Schematic Picture of Radio and X-ray Emission

- **Our model for the typical active star!**

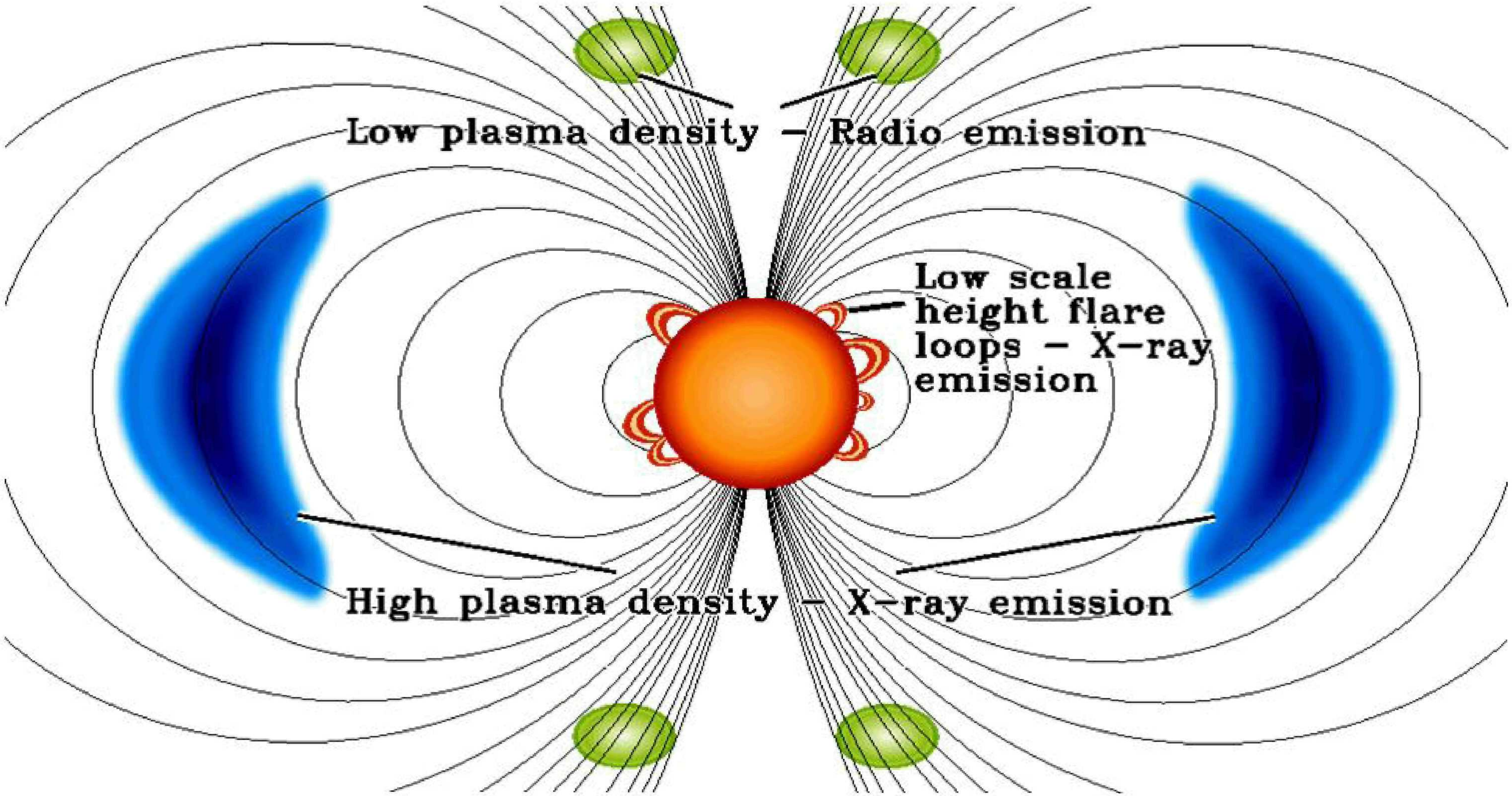

Planetary Magnetospheres

All solar system planets with strong magnetic fields (Jupiter, Saturn, Uranus, Neptune, and Earth) also produce intense radio emission – with frequencies close to the cyclotron frequency.

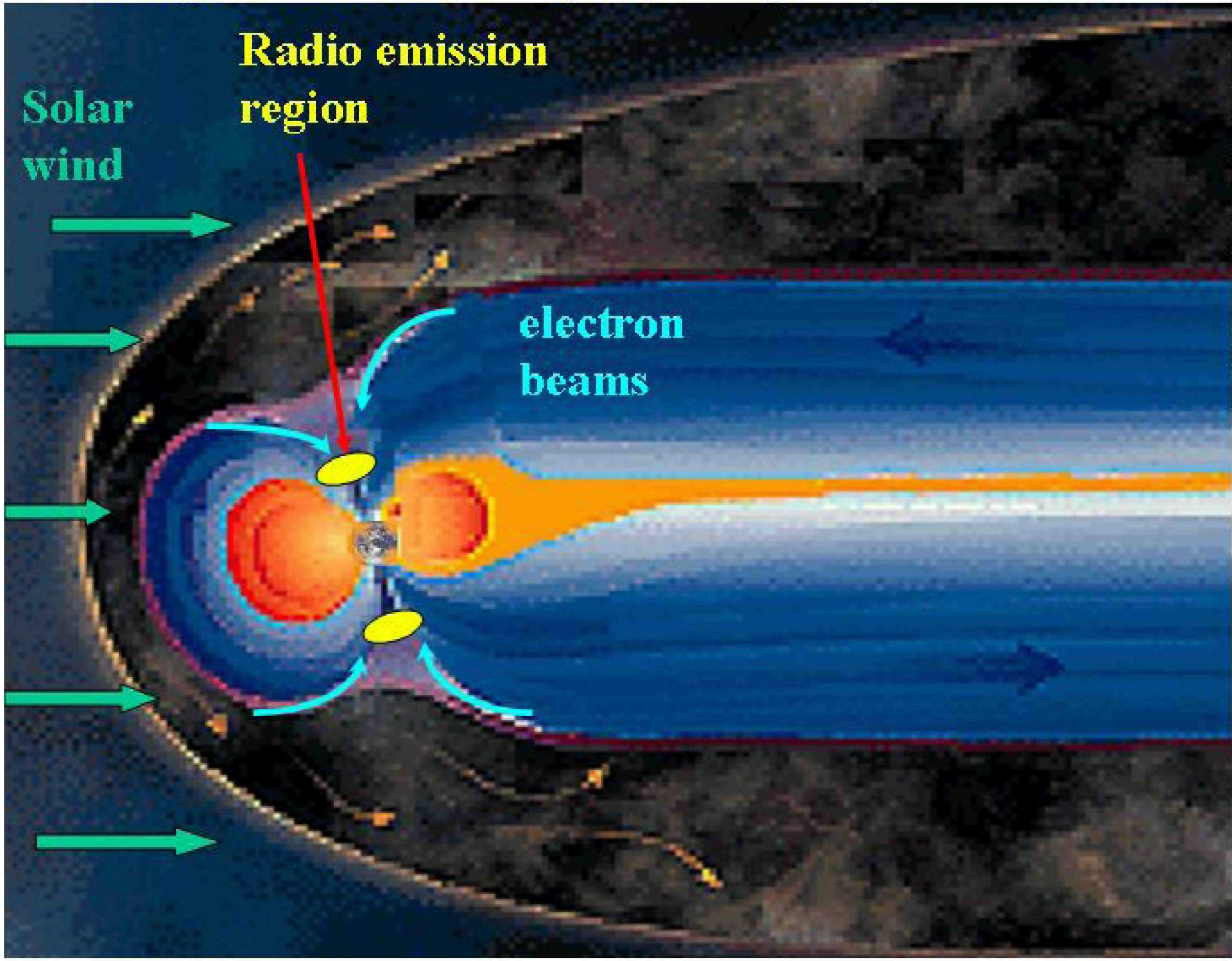

Planetary Aurora

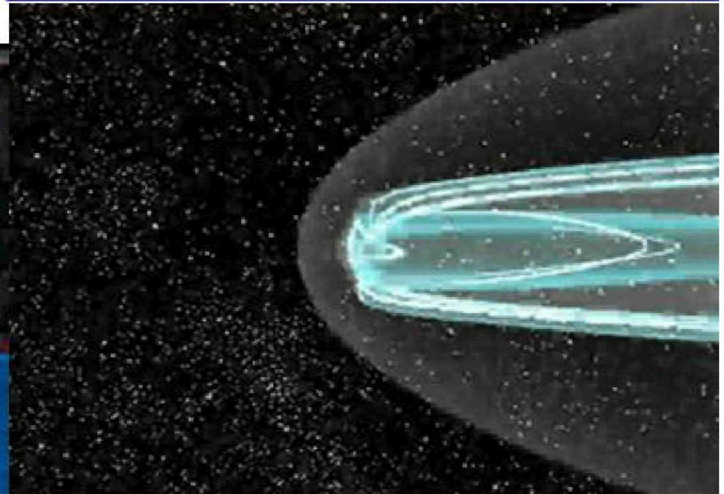

Animation courtesy of NASA

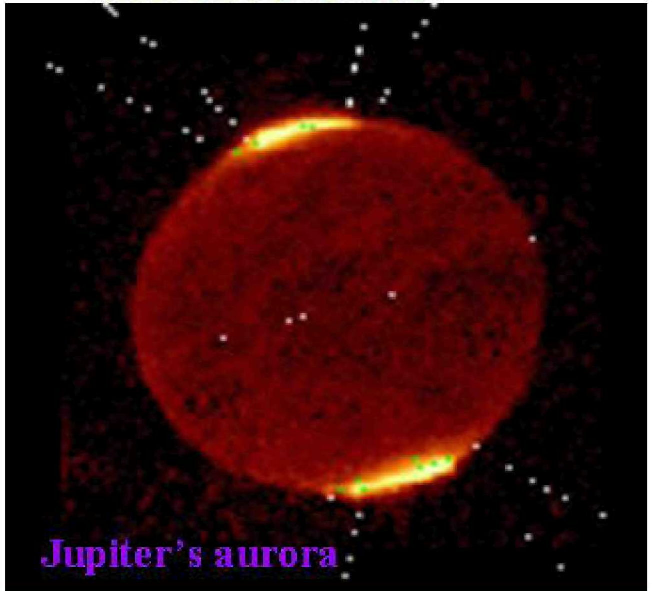

Planetary Radio Emission

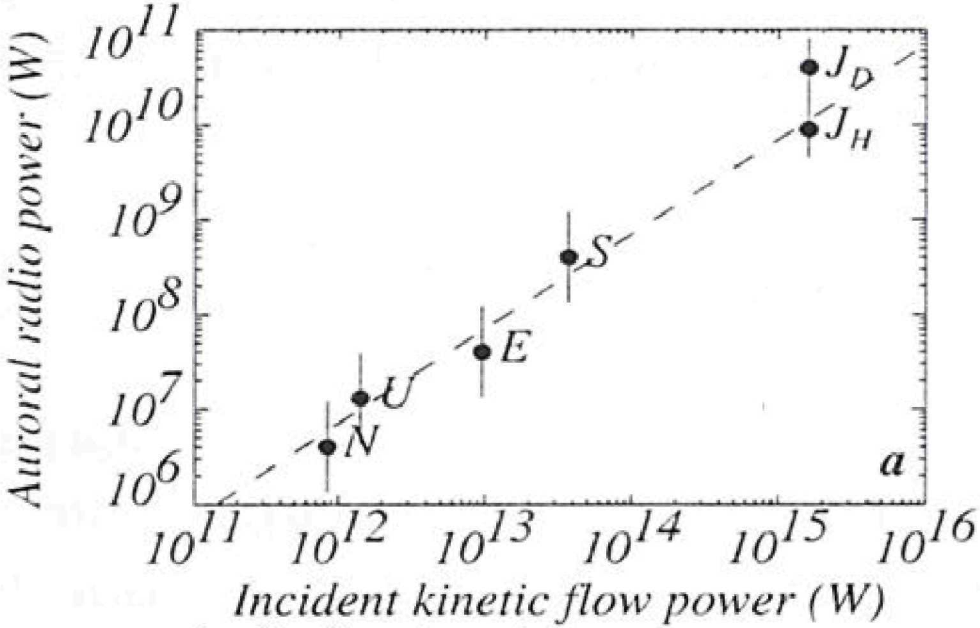

i.e. **due to solar wind ram pressure**

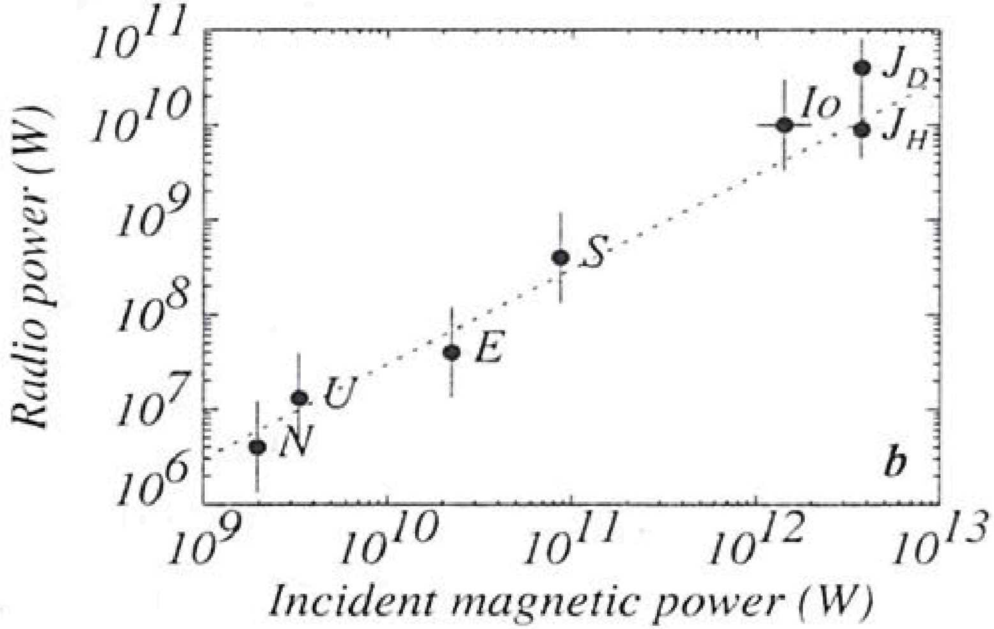

- **(a)** Initial radio Bode's law for the auroral radio emissions of the five radio planets (Earth, Jupiter, Saturn, Uranus and Neptune) (Desch and Kaiser, 1984; Zarka, 1992). J_D and J_H correspond to the decameter and hectometer Jovian components, respectively. The dashed line has a slope of 1 with a proportionality constant of 7.10^{-6}. Error bars correspond to the typical uncertainties in the determination of average auroral radio powers. **(b)** Magnetic radio Bode's law with auroral and Io-induced emissions (see text). The dotted line has a slope of 1 with a constant of 3.10^{-3}.

Electron acceleration in the aurora

- **DE-1 at 11000 km over the polar cap** [Menietti & Burch, JGR, 90, 5345, 1985]

Observations of auroral electrons

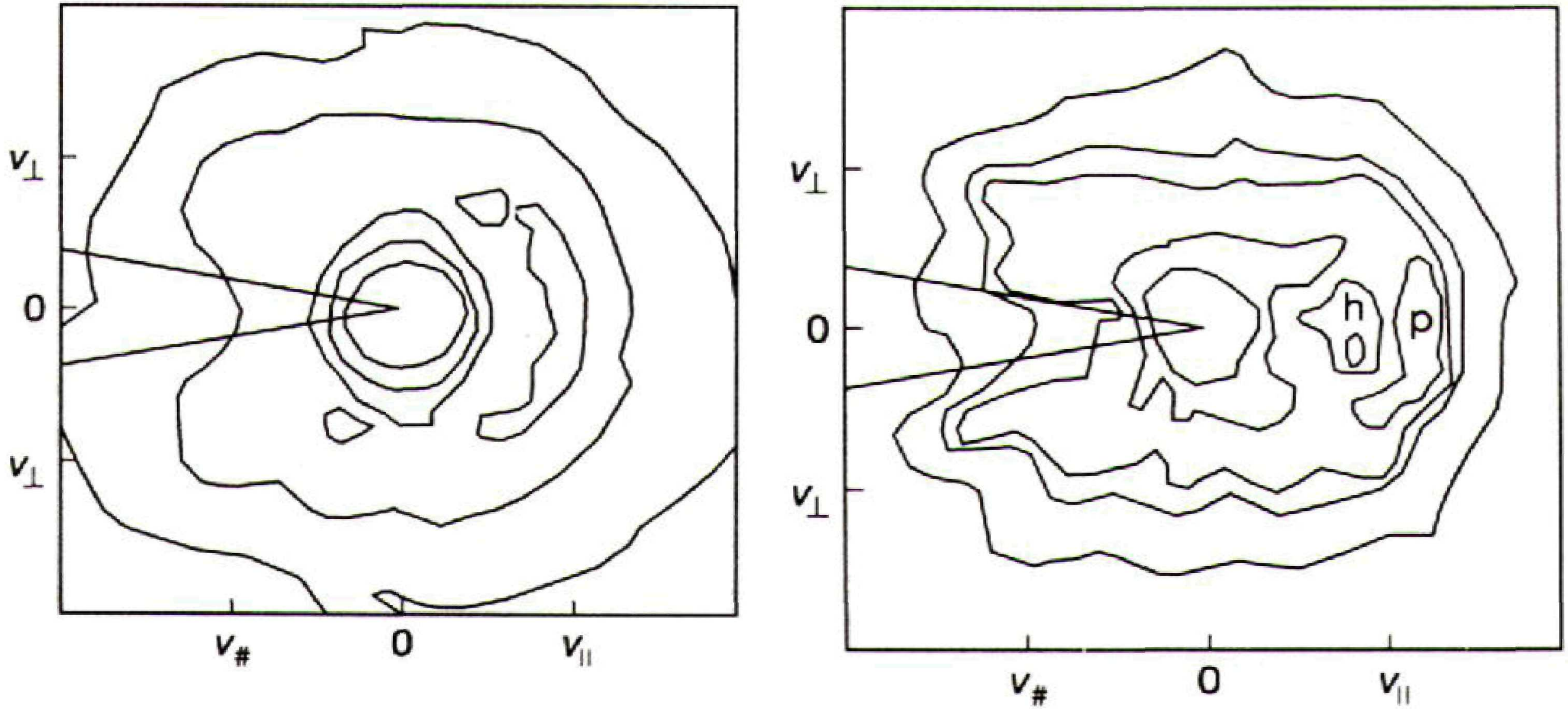

Electron distribution with a crescent shaped peak in the downward direction

A crescent-shaped peak (p) with the addition of a field-aligned hollow (h).

Observations of auroral electrons

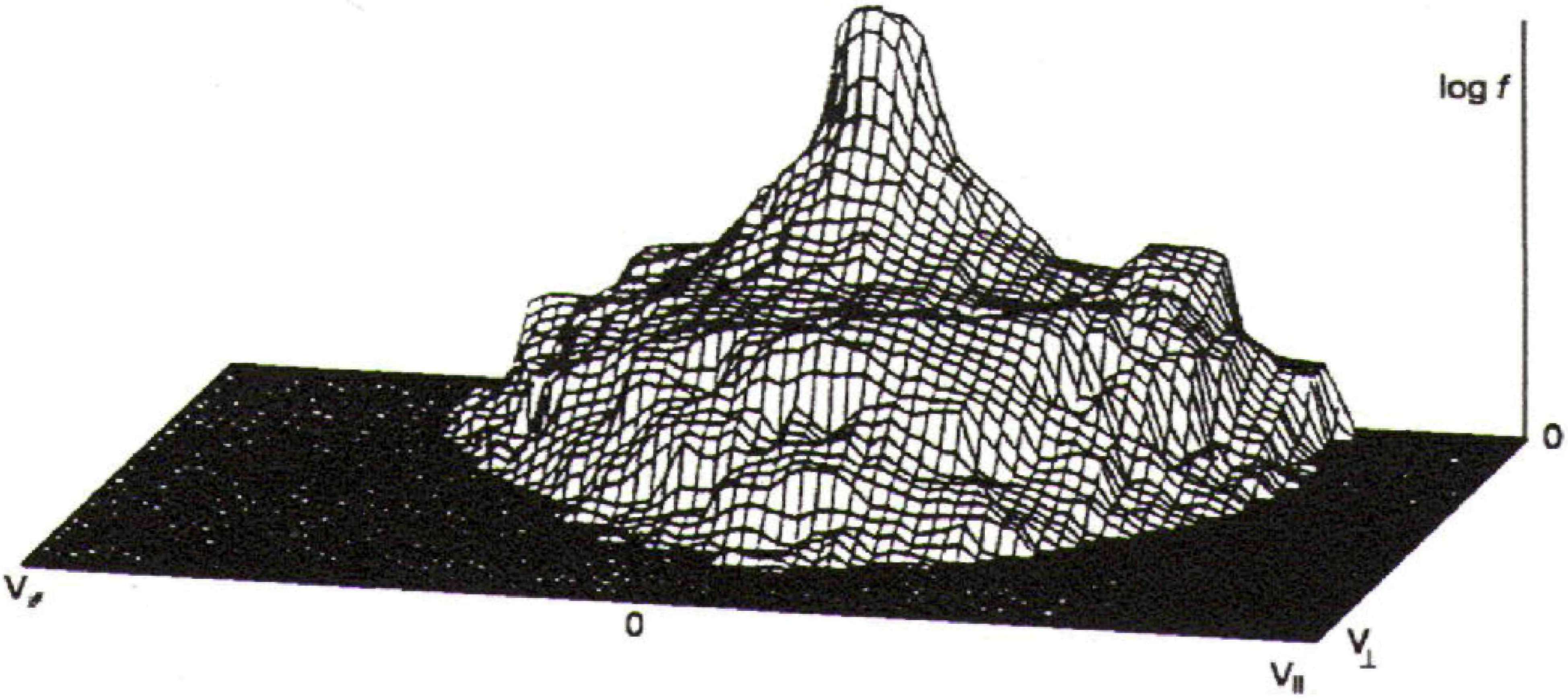

Mountain-like surface plot of an auroral electron distribution exhibiting a distinct beam at the edge of a relatively broad plateau.

FAST Observations of electron distributions in the AKR source region

- **Delory *et al.* - GRL <u>25</u> (12), 2069-2072, 1998.**

  Delory *et al.* reported on high time-resolution 3-D observations of electron distributions recorded when FAST was actually within the AKR source region. In general, the electron distributions show a broad plateau over a wide range of pitch angles.

They presented computer simulations of the evolution of the electron distribution which assumed plasma conditions similar to those observed by FAST and which show similar results to those observed.

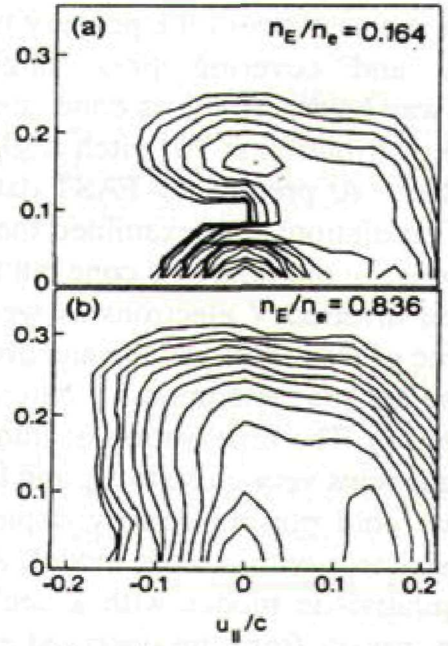

Figure 3. The results of numerical simulations shown in Figure 15 of the work by *Winglee and Pritchett* [1986]. The distribution in (a) has been stabilized by electrostatic waves; (b) shows diffusion due to AKR growth when the energetic electrons dominate the plasma.

CCLRC Rutherford Appleton Laboratory

FAST Observations - Delory *et al.* GRL, 25(12), 2069, 1998

- The observed radio emission from UV Ceti is actually remarkably similar in form to the Earth's AKR emission [AKR = Auroral Kilometric Radiation]. Here are some measurements of the electron distribution functions seen in the AKR formation region.

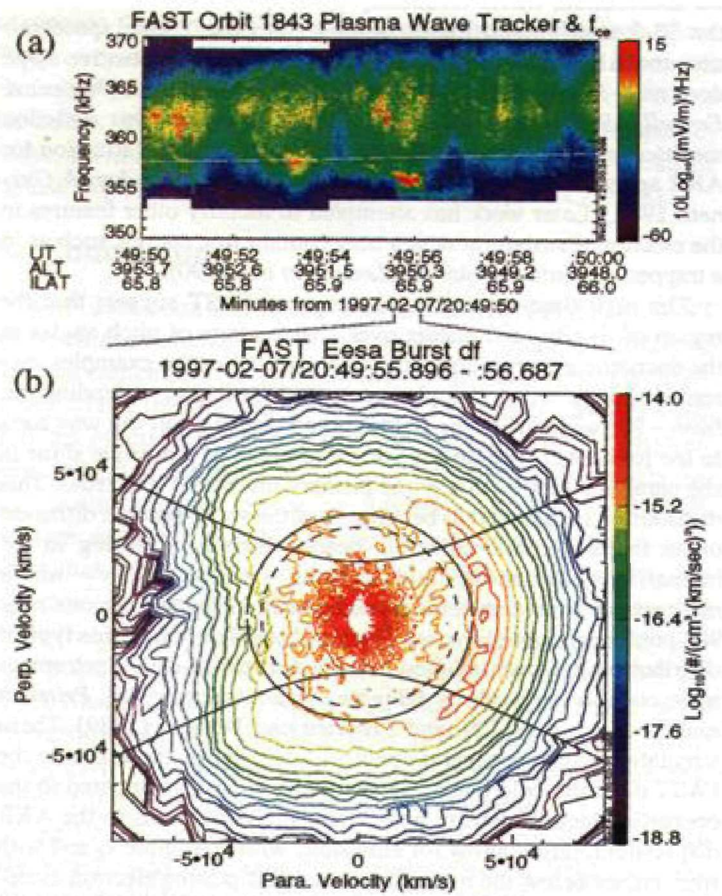

Figure 1. (a) Plasma Wave Tracker data and (b) electron contour plot for orbit 1843. The solid lines represent boundaries for adiabatic motion of electrons (see *Chiu and Schulz* [1978]), while the dotted inner circle shows the resonance condition with $k_{\parallel} = 0$ in Equation (1) for the AKR burst near ~20:49:56 UT.

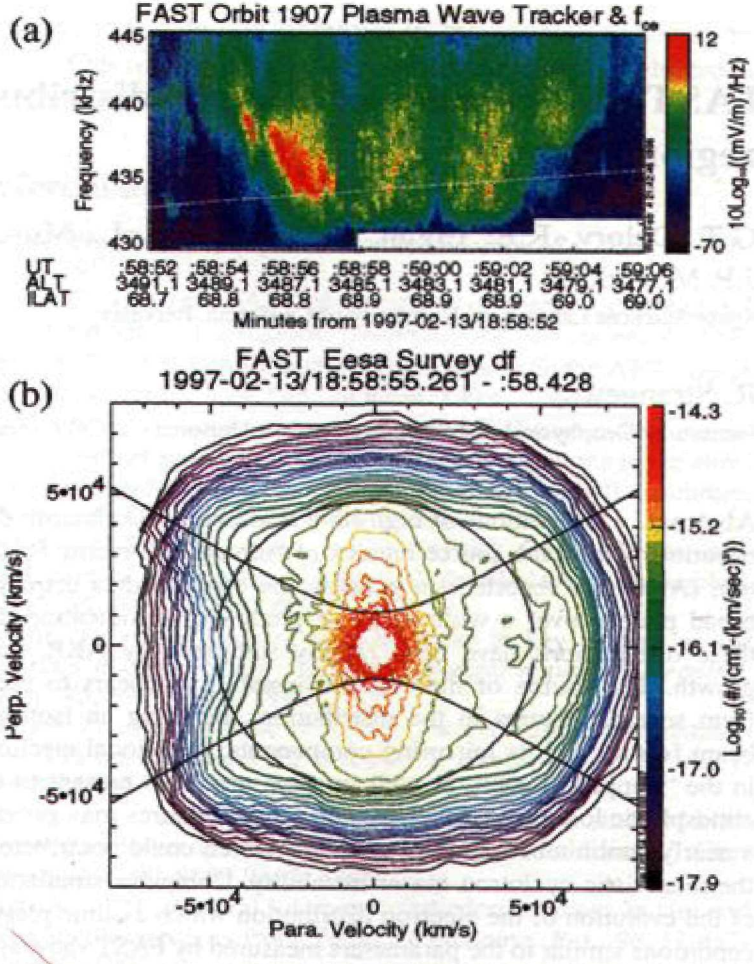

Figure 2. (a) AKR spectra measured using the Plasma Wave Tracker instrument and (b) electron contour plots obtained in this source region for FAST orbit 1907.

Strangeway *et al.* 2001 – FAST Data "Cartoon"

The figure shows an electron distribution function acquired by FAST within the aurural density cavity (see later). This is the region where the auroral kilometric radiation (AKR) is generated.

The figure also shows the envisaged flow of energy. Parallel energy gained from the electric field (stage 1) is converted to perpendicular energy by the mirror force (stage 2). This energy is then available for the generation of AKR and diffusion to lower perpendicular energy (stage 3).

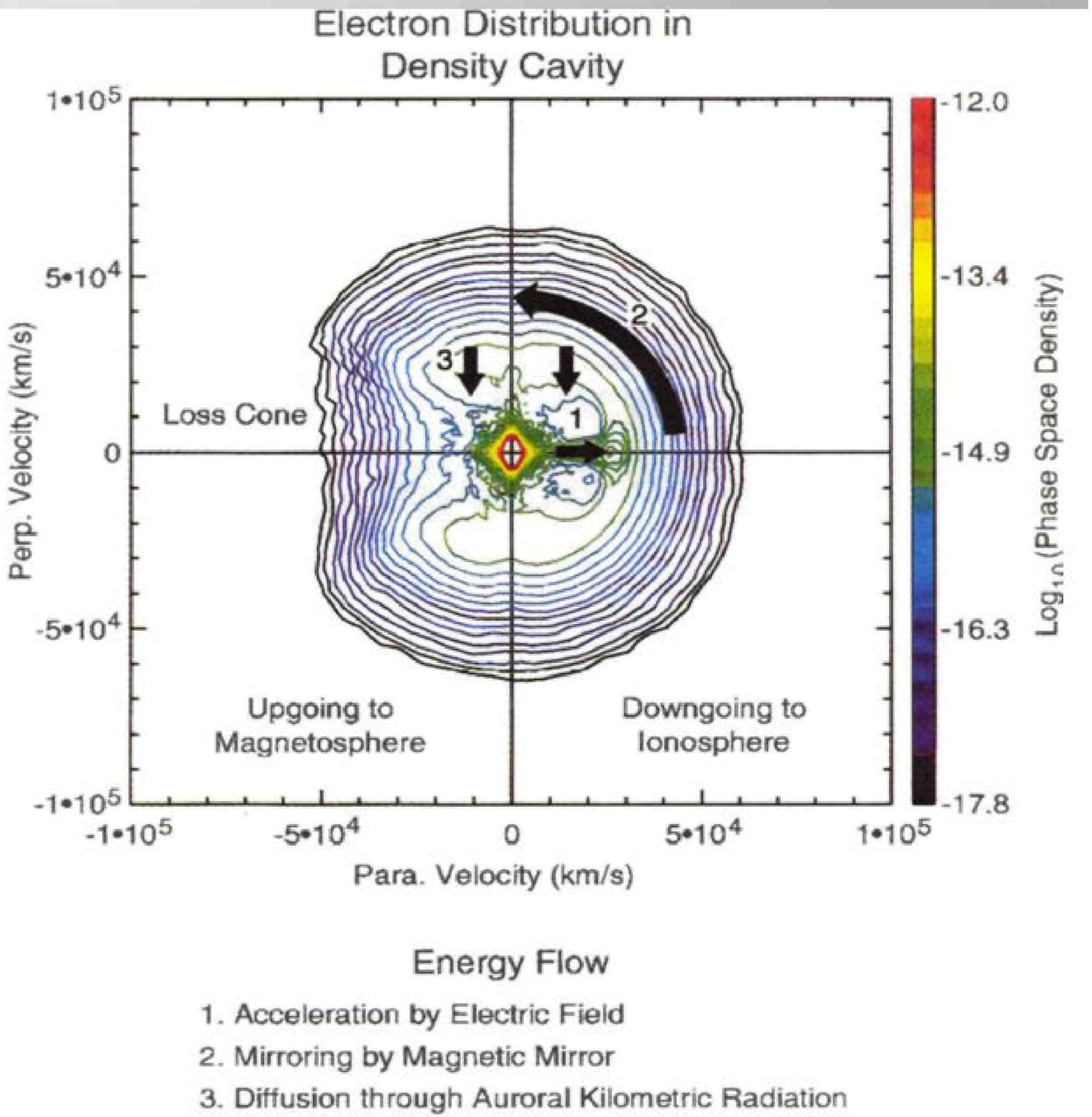

Auroral Kilometric Radiation

- Emission from low density channels in auroral region.
- Narrow bandwidth at frequency just below electron cyclotron frequency.
- Polarised in X mode and generated near perpendicular to magnetic field.

Explanations have tended to focus on loss-cone instability, but we suggest cyclotron instability associated with formation of "horseshoe" distribution in beams.

Bandwidth and Polarization

CCLRC Rutherford Appleton Laboratory

- The bandwidth is also extremely narrow, from the figure estimated to be about 0.05% or around 200 Hz.
- Also in agreement with observations is the polarization in the R-X mode.

$$\mu_0 = \frac{1}{2} m V_\perp^2 \Big/ B_0$$

SATURATION

Non-linear saturation by decreasing μ_0

i.e. the opening angle and thermally spreading the beam.

Horseshoe Formation

Field aligned electron beams naturally form a horseshoe distribution as they move into stronger magnetic field regions. The adiabatic invariance $v_\perp^2/B$ = constant causes the electrons to lose parallel energy and increase their perpendicular energy producing the characteristic horseshoe distribution with $\partial f_e / \partial v_\perp > 0$.

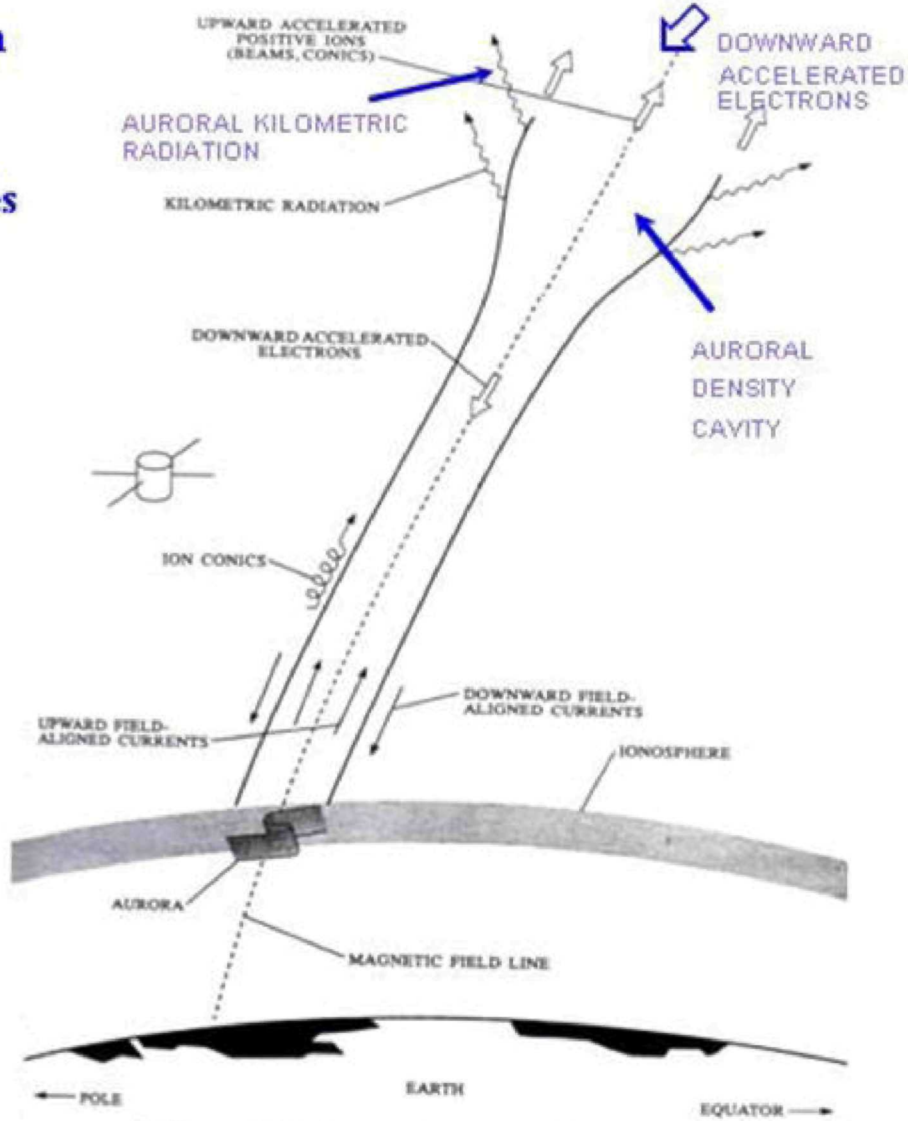

Schematic illustrating the terrestrial auroral process.

Requirements

$$\frac{\partial f_e}{\partial v_\perp} > 0 \qquad \Omega_c > \omega_{pe}$$

where $\Omega_c = \dfrac{eB}{m_e}$, $\omega_{pe} = \left(\dfrac{n_0 e^2}{m_e \varepsilon_0}\right)^{1/2}$

Low density cold background such that $n_H > n_C$

Evolution of an auroral electron energy beam distribution (Bryant and Perry, JGR, 100, 23711, 1995)

A-H show different altitudes evenly space between 24000 and 1000 km. The velocity range is from 0 up to 80 km/s.

Acceleration was assumed to take place for 2000 km immediately below A. This acceleration produces a field-aligned beam at B which steadily widens to become the crescent-shaped feature in G and then widens even further to become almost isotropic in H.

A crucial feature of the wave theory is the symmetry outside the loss cone about the zero parallel velocity axis, revealing that the conic is simply the magnetically mirrored outer part of the down-going beam.

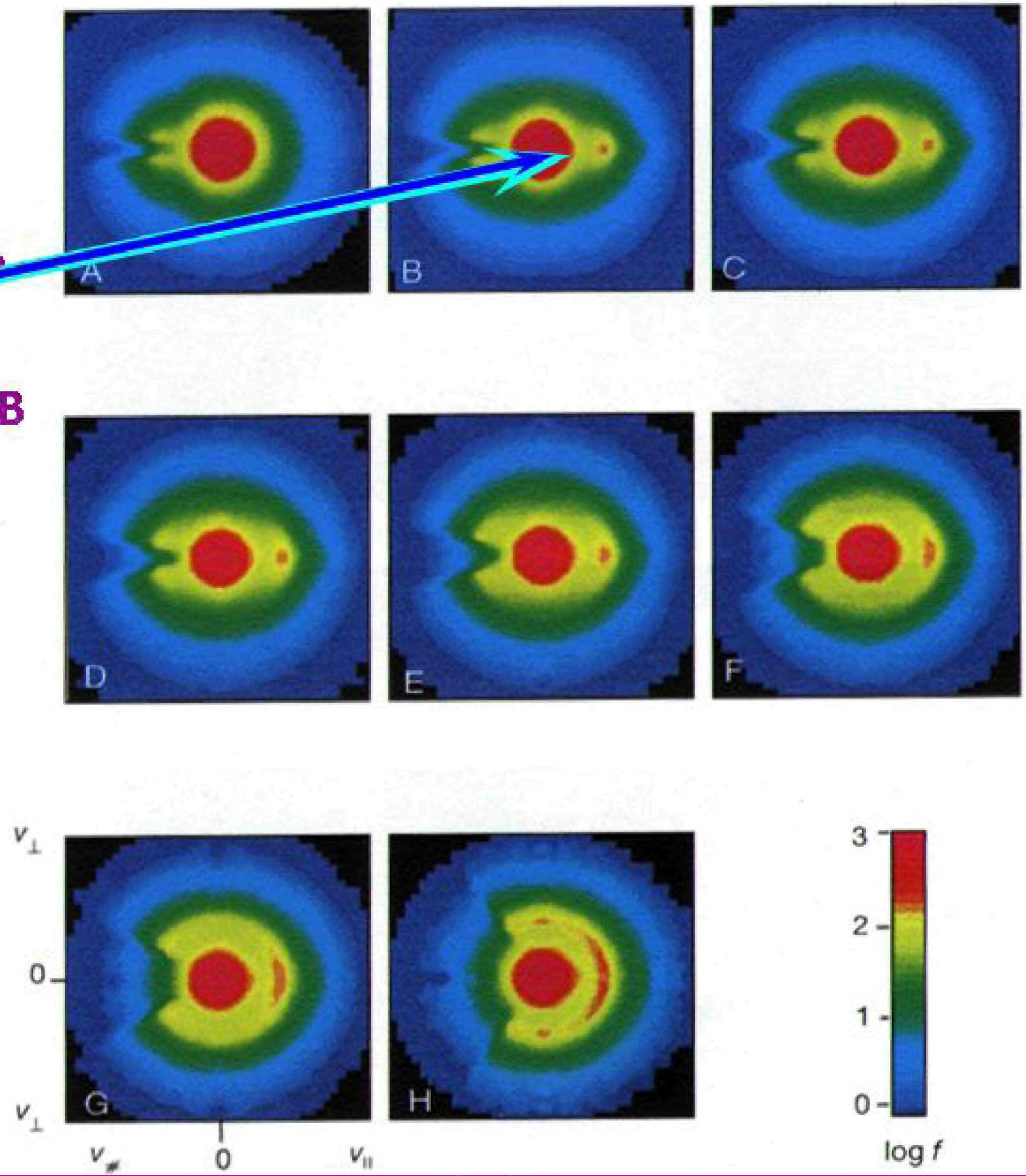

Formation of horseshoe distribution.

Beam with thermal spread moving down converging magnetic field lines. Conservation of magnetic moment means that particles lose parallel energy and gain perpendicular energy. Here, we show the evolution of beam with initial Maxwellian spread, moving into increasing B field.

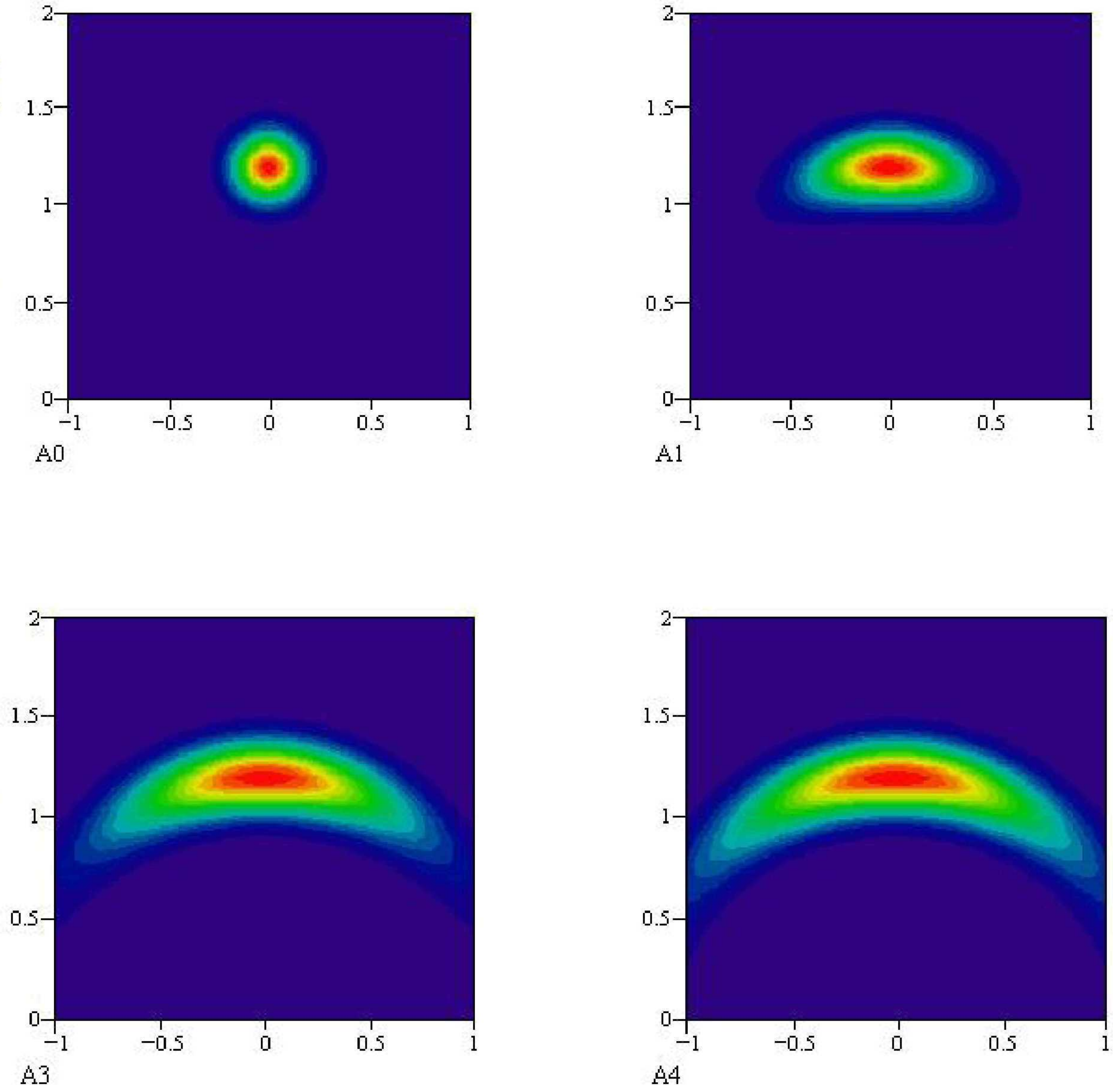

Cyclotron resonance condition:

$$\omega - \frac{n\omega_{ce}}{\gamma} - k_{\|} v_{\|} = 0$$

For small parallel wavenumber, resonant frequency is shifted below cyclotron frequency by an amount dependent on the particle energy.

The effect of cyclotron resonance is to produce diffusion of the particle in velocity space, mainly in the perpendicular degree of freedom (entirely in the perpendicular direction for propagation normal to the field). This follows from momentum conservation.

Theory

Dielectric tensor element (from Stix)

$$\varepsilon_{xx} = \frac{\omega_{pe}^2}{\omega\omega_{ce}} \sum_n \int_0^\infty 2\pi p_\perp dp_\perp \int_{-\infty}^\infty dp_\parallel \frac{\omega_{ce}/\gamma}{\omega - k_\parallel v_\parallel - n\omega_{ce}/\gamma}$$

$$\times \frac{n^2 J_n^2(z)}{z^2} p_\perp \left[\frac{\partial f_0}{\partial p_\perp} + \frac{k_\parallel}{\omega}\left(v_\perp \frac{\partial f_0}{\partial p_\parallel} - v_\parallel \frac{\partial f_0}{\partial p_\perp}\right)\right]$$

with

$$z = \frac{k_\perp v_\perp \gamma}{\omega_{ce}}$$

Some Assumptions

Make following simplifications:-

- Put $k_{\|} = 0$.
- Use cold plasma approximation for real part.
- Take account of imaginary part from n =1 term, assuming radiation near fundamental cyclotron frequency.
- Assume z small, (effectively saying that perpendicular velocity spread << c).

This allows us to make the approximation

$$\frac{J_1^2(z)}{z^2} \approx \frac{1}{4}$$

CCLRC Rutherford Appleton Laboratory

Modelling the Growth Rate of electron cyclotron

$$\mathrm{Im}(\varepsilon_{xx}) = -\frac{1}{2}\frac{\omega_p^2}{\omega\omega_{ce}}\pi^2\int_{-1}^{1}(1-\mu^2)P(1+P^2)\times\left(\frac{\partial f_0}{\partial P}-\frac{\mu}{P}\frac{\partial f_0}{\partial\mu}\right)d\mu$$

with $P=\sqrt{\frac{\omega_{ce}^2}{\omega^2}-1}$ (resonant momentum in units of mc).

We then use $n_\perp = \sqrt{\frac{\varepsilon_{xx}^2-\varepsilon_{xy}^2}{\varepsilon_{xx}}}$

to find the perpendicular refractive index. A negative imaginary part corresponds to spatial growth of the wave.

Results below are given for $\frac{\omega_{pe}}{\omega_{ce}}=0.1$

Modelling the Growth Rate of electron cyclotron

- The spatial growth rate can be obtained by solving

$$\frac{n\,c\,\mathrm{Im}\,k}{\Omega_{e0}} = -\frac{\alpha(\omega-\Omega_{c0})^2(2\Omega_{c0}^2-\omega_{pe}^2)^2}{\omega_p^4\Omega_{c0}^2}$$

where n is the refractive index and

$$\alpha = \frac{1}{4}\frac{\omega_{pe}^2}{\Omega_{c0}^2}2\pi^2 m^2 c^2\int_{-1}^{1} d\mu(1-\mu^2)p^2\left(\frac{\partial f_e}{\partial p}-\frac{\mu}{p}\frac{\partial f_e}{\partial \mu}\right)\Bigg|_{p=p_0}$$

is represented in spherical polar co-ordinates (p, μ, φ) with θ replaced by $\mu = \cos\theta = p_{\|}/p$

and the resonant momentum $p_0 = mc\,(2(\Omega_{c0}-\omega)/\Omega_{c0})^{1/2}$

The horseshoe distribution $f(p, \mu) = F(p)\,g(\mu)$

$$\alpha = \Gamma\left(P\frac{\partial F}{\partial p}+Q\frac{F}{p}\right)\Bigg|_{p=p_0}$$

destabilizing stabilizing

Modelling the Growth Rate of electron cyclotron

where

$$P = \int_{-1}^{1} \left(1 - \mu^2\right) g(\mu) d\mu$$

$$Q = \int_{-1}^{1} \left(1 - 3\mu^2\right) g(\mu) d\mu$$

The first term in α results in emission of the waves if

$\partial F/\partial p$ is +ve at the resonant momentum.

The second term is -ve and goes to zero if g becomes uniform on the interval [-1, 1]

- The beam requires the correct $\perp$ spread to trigger the emission of AKR

CCLRC Rutherford Appleton Laboratory

Numerical Solutions

- A test particle description of the surfatron acceleration model can easily be described using relativistic equations for the particle. Consider a magnetic field in the z direction and a wave with a longitudinal electric field moving in the $\boldsymbol{y}$ direction. The equations of motion for an electron are

$$\frac{dp_x}{dt} = -\frac{eBp_y}{m_0\gamma} \qquad \frac{dp_y}{dt} = \frac{eBp_x}{m_0\gamma} - eE\sin(ky - \omega t) \qquad \frac{dy}{dt} = \frac{p_y}{m_0\gamma}$$

where m_0 is the electron rest mass, p_i is the particles momentum ($= \gamma m_0 v_i$).

- If we switch to normalised units, these equations simplify to

$$\frac{dp_x}{dt} = -\frac{p_y}{\gamma} \qquad \frac{dp_y}{dt} = \frac{p_x}{\gamma} - \beta\sin(ky) \qquad \frac{dy}{dt} = \frac{p_y}{\gamma} - \alpha$$

where $\alpha = \omega/k$ the wave phase speed and $\beta = eE/mc\Omega_{eo}$ and (Ω_{eo} is the non-relativistic cyclotron frequency)

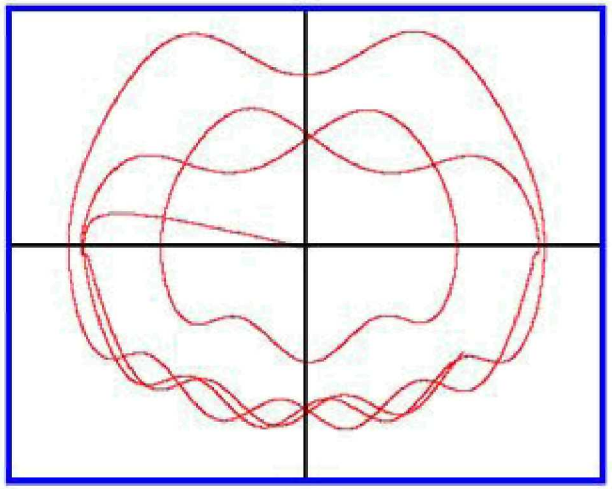

Numerical solution of equations for a wave speed of $\alpha = \omega k = 0.3$, $k = 0.2$, and $\beta = 1.045$, depicting phase space diagram for x and y components of the perpendicular momenta which form a ring perpendicular to the magnetic field.

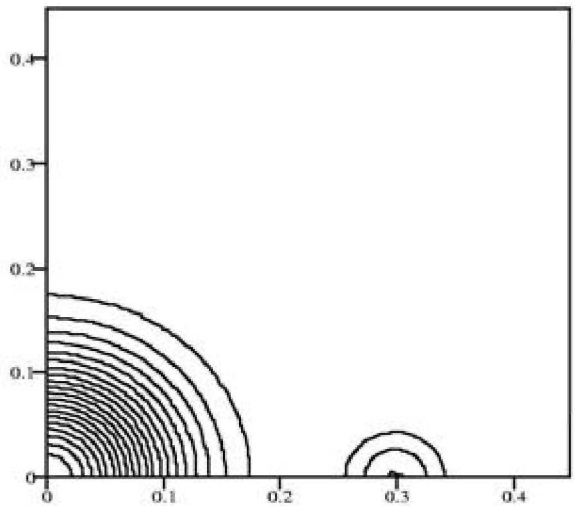

Contour plot in momentum space of the electron momentum components depicting a background Maxwellian and a perpendicular ring distribution.

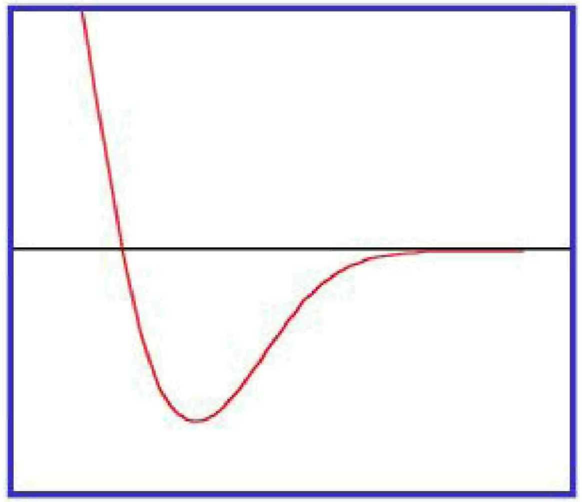

Spatial growth rate of R-X mode for the ring distribution

Modelling the Growth Rate of electron cyclotron

- **Model Input**

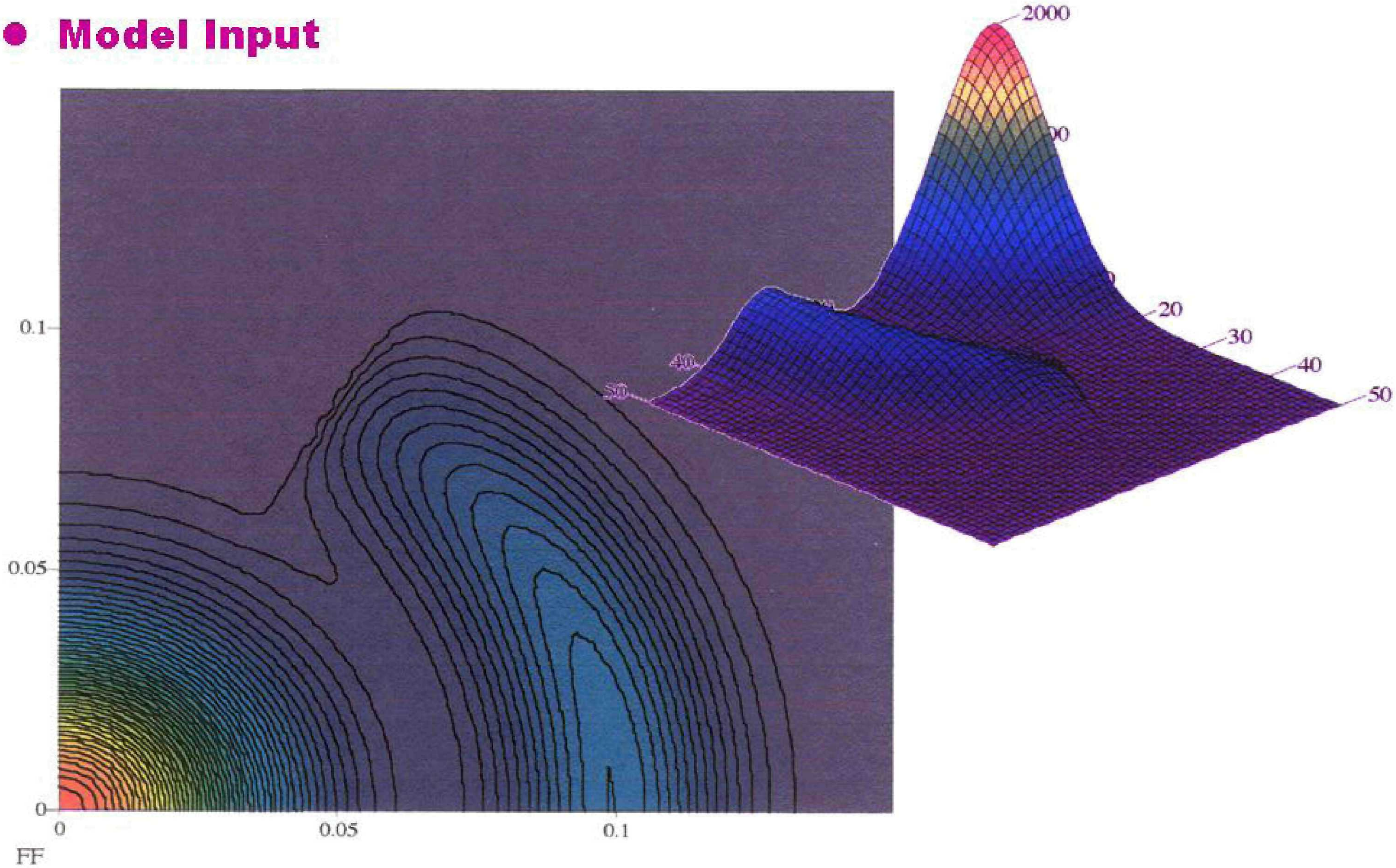

Growth Rate of Electron Cyclotron

- **AKR in Auroral Zone**

Consider a horseshoe centred on $p_{\|} = 0.1\ m_e c$ - i.e. a 5 keV beam, with a thermal width of 0.02 $m_e c$ and an opening angle of $\mu_0 = 0.5$ moving in a low density Maxwellian plasma with $T_e = 312$ eV,

$\omega_p/\Omega_{ce} = 1/40.$

A typical convective growth length across B $L_c = 2\pi/\mathrm{Im}\ k_\perp$ is 10 λ. For a cyclotron frequency of 440 kHz the convective growth distance is of order 5 km allowing many e-foldings within the auroral cavity which has a latitudinal width of about 100 km. The growth rate decreases for increasing μ_0 and increasing thermal width of the horseshoe distribution.

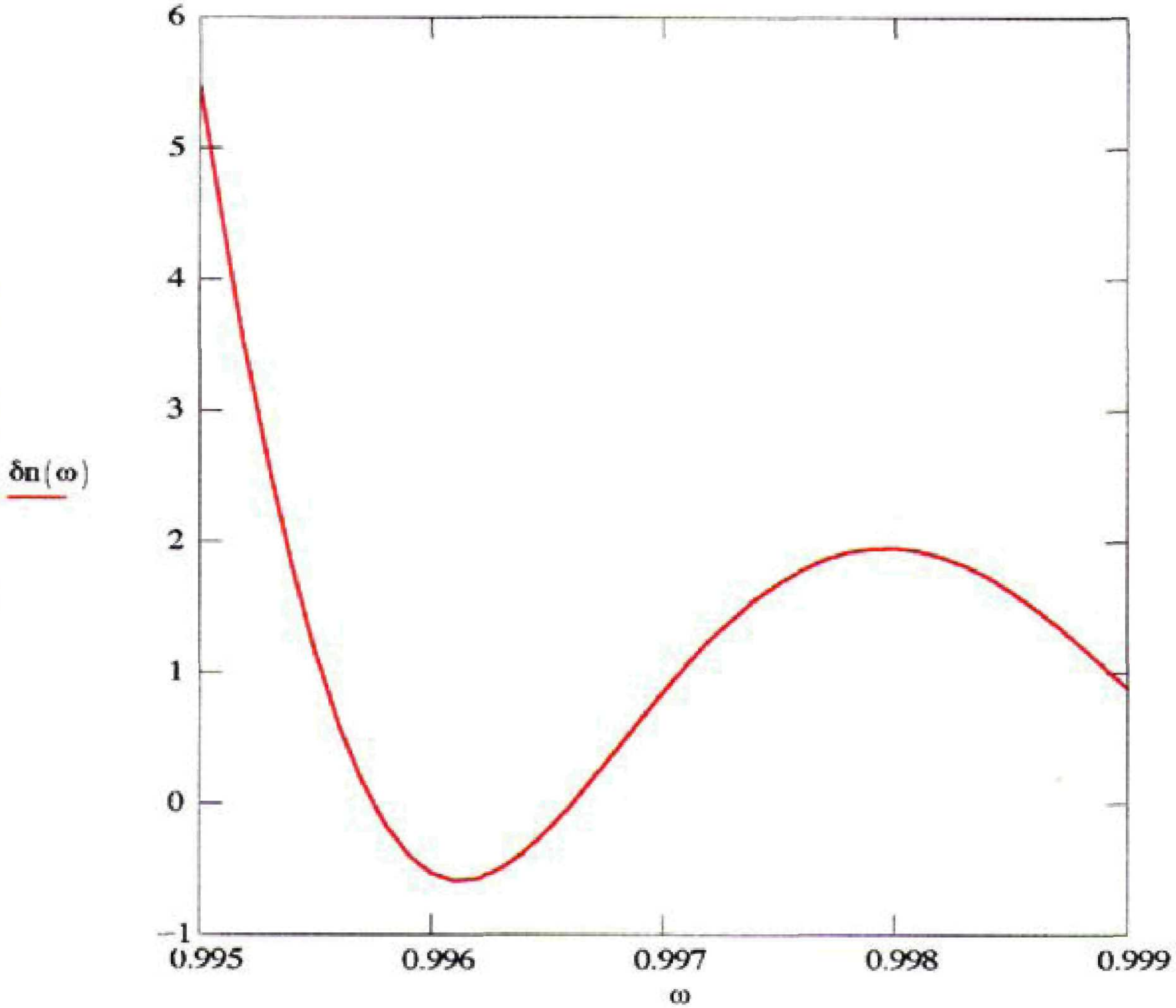

Simulation Results

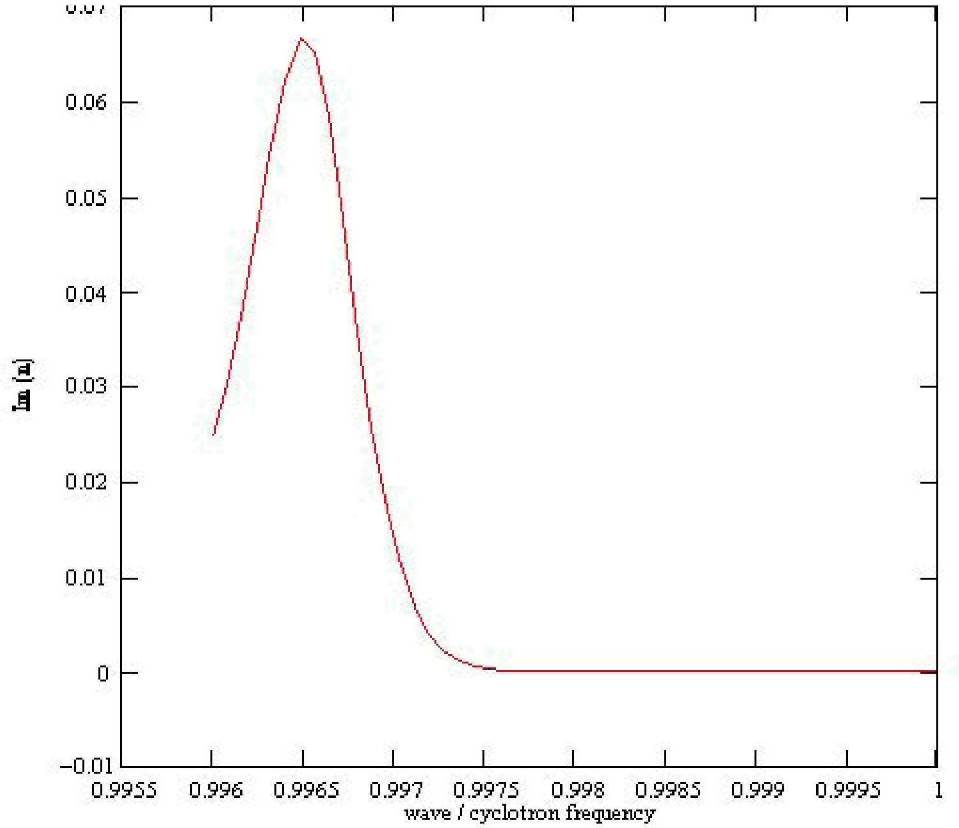

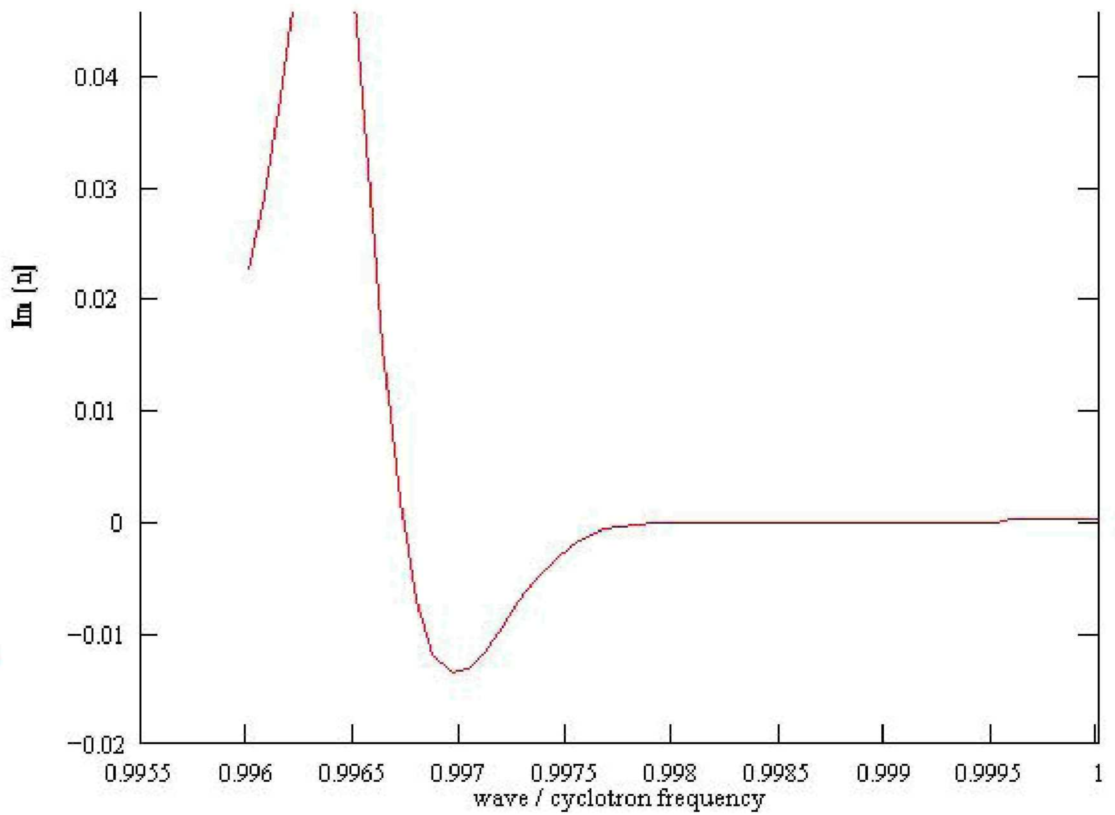

The imaginary part of the refractive index as a function of frequency for a mean beam energy of 5 keV and a thermal spread of 50 eV. The magnetic field ratio is 3 on the left and 5 on the right.

Main Features of Instability

- High spatial growth rate when magnetic field ratio becomes high enough.
- Radiation from a given region is in a narrow bandwidth below the local electron cyclotron frequency.
- For densities in the range of interest, the instability growth rate decreases with density, so low density regions are favoured, in agreement with the observation that emission takes place from low density channels.

CCLRC Rutherford Appleton Laboratory

Why the X-mode and not the O-mode?

The tensor elements which enter into the X-mode dispersion relation appear to zero order in the expansion in z of the Bessel functions.

For the O-mode a non-zero imaginary part appears at order z^2, This means that the growth rate is proportional to (thermal spread of beam/c)^2.

Why generation close to the perpendicular?

Instability when resonant momentum runs around inner edge of horseshoe. If there is a parallel velocity wavenumber component, resonant momentum line cuts across horseshoe.

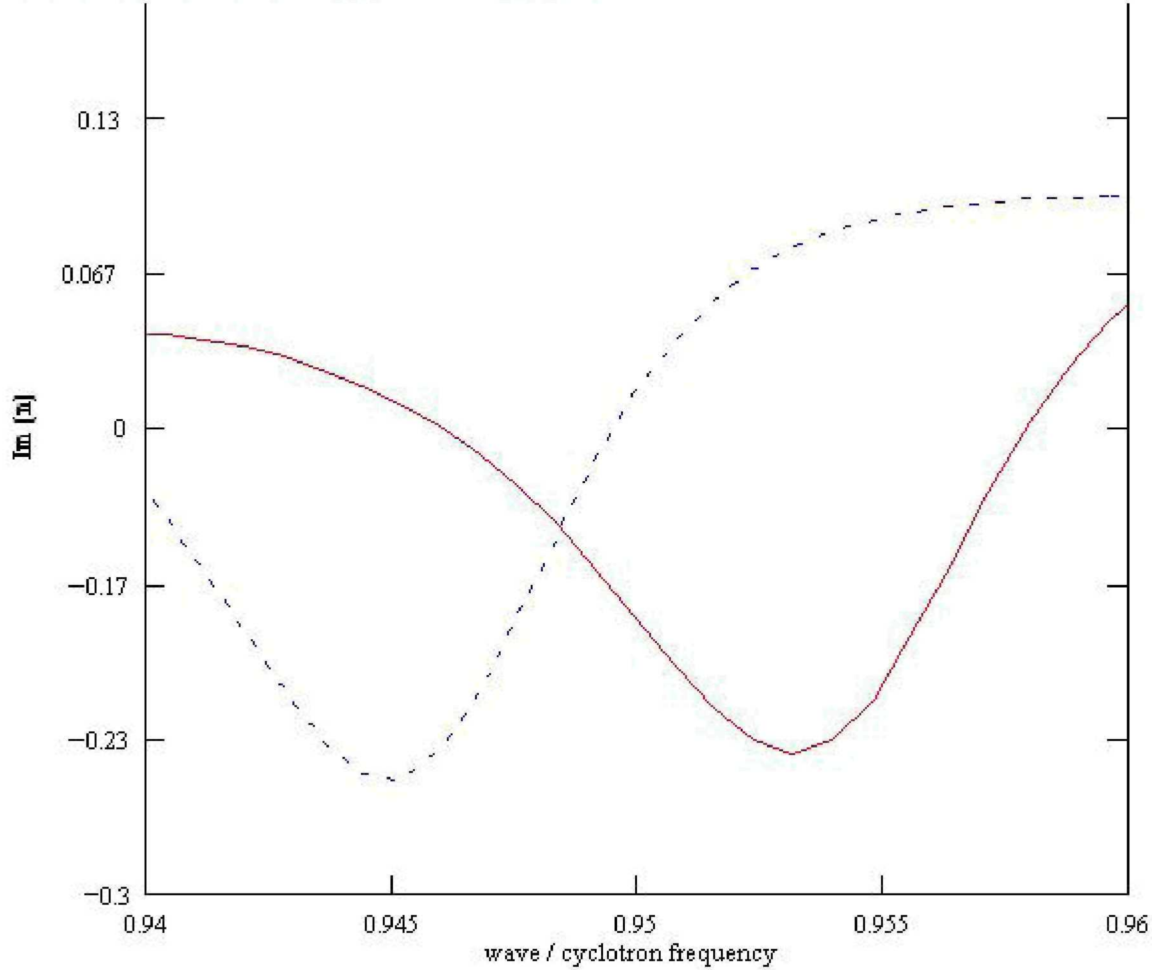

Graph shows reduction in growth rate for propagation a few degrees off perpendicular.

Problem with Loss-Cone Mechanism

- A major problem with explaining the AKR by a loss-cone instability is accounting for the power output.
- What sort of power might be available from our mechanism?
- An upper limit can be obtained by assuming complete quasilinear saturation of the instability, so the horseshoe is flattened out in the perpendicular direction.

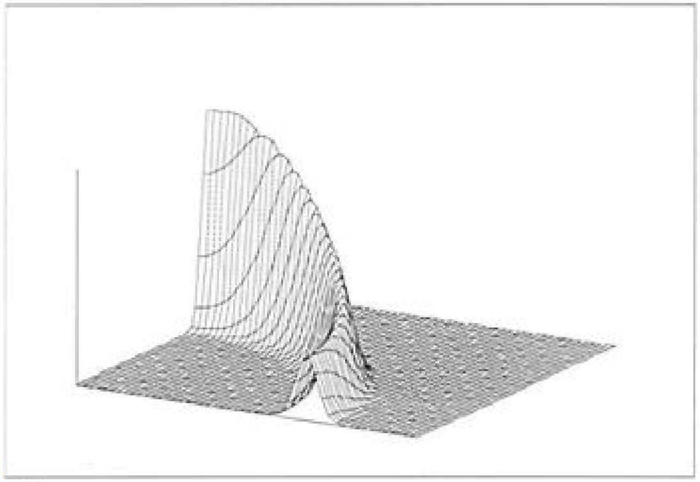

AA

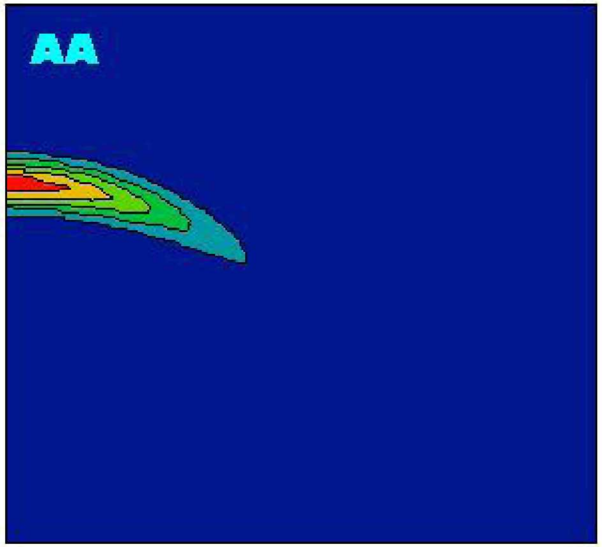

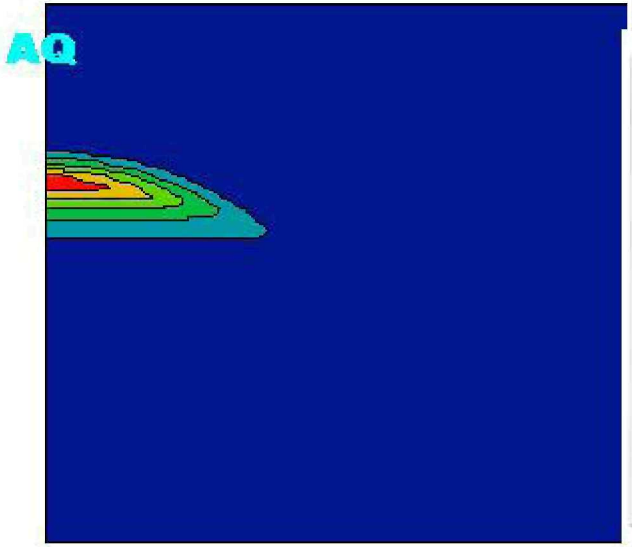

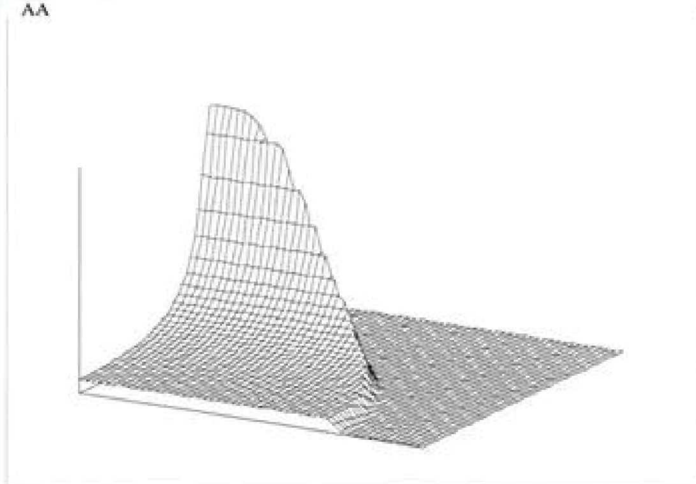

AQ

With magnetic field increase by a factor around 50, this gives a the fraction of the power transferred to the wave to be around 10%.
The power needed to explain observed levels of AKR is of the order of a few percent of the beam energy at most.

Applications

There are many situations in space and astrophysics where a combination of particle beams and converging magnetic fields exists.

One application we have looked at is to emission from the star UV Ceti - see "*Can late-type active stars be explained by a dipole magnetic trap*", B J Kellett *et al.*, Mon. Not. R Astron. Soc. 329, 102 (2002).

Maser radiation generated in magnetic traps – Bingham, Cairns, *Phys. Fluids*, 7, 3089, 2000.

Application to astrophysical shocks – Bingham *et al.*, *Ap.J.*, 2003 (in press).

Main feature of interest - transient X-ray emission from hot electrons followed by bursts of radio emission.

Laboratory Application

Theory and observations from the auroral regions suggest that this instability can be reasonably efficient in converting beam energy to radiation.

It depends only on dimensionless parameters like the ratios of the various characteristic frequencies and the factor by which the magnetic field increases.

Can it be scaled to be the basis of a useful device for generating high power, high frequency radiation in the laboratory?

Joint research programme between Universities of Strathclyde, St Andrews and the Rutherford Laboratory.

Cyclotron Maser Radiation

CCLRC
Rutherford Appleton Laboratory

UV Ceti

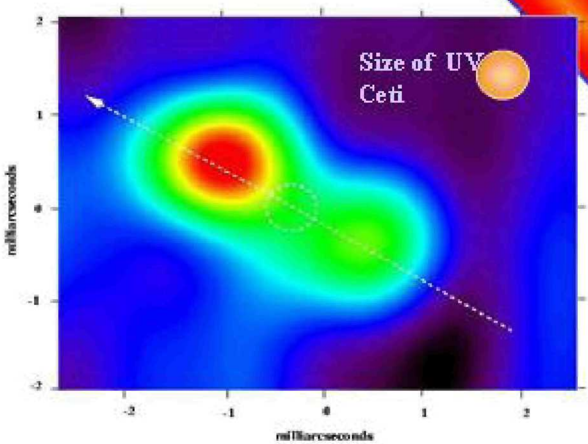

Planetary Aurora

How "blue sky" research can lead directly to practical laboratory experiments

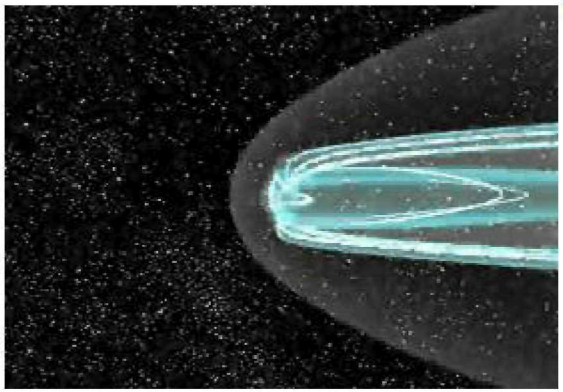

Animation courtesy of NASA

Laboratory Experiment

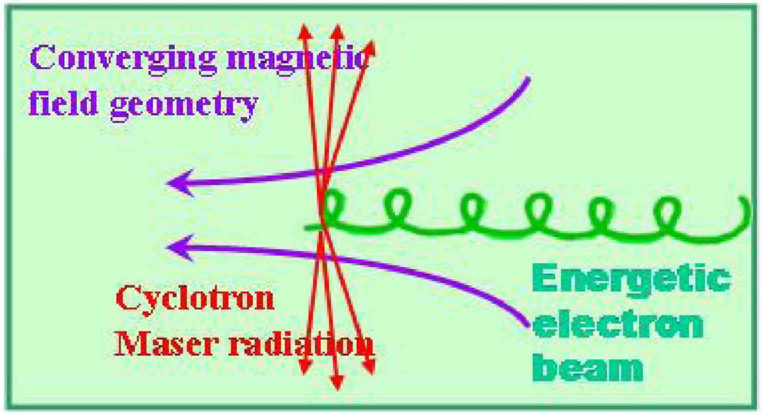

10 kW e-beam ⇒ 1 kW Radiation
At the cyclotron frequency

Radio Emission Mechanism – Everywhere!?

- **Polarised radio emission from active stars (and the Sun!)**
- **Kilometric and Decametric radio emission from Earth, Jupiter, etc.**
- **Pulsar radio emission mechanism?**
  - Newly discovered binary pulsar is the perfect "laboratory" for studying this!
- **Highest Energy Cosmic ray air showers?**
- **Laboratory!**

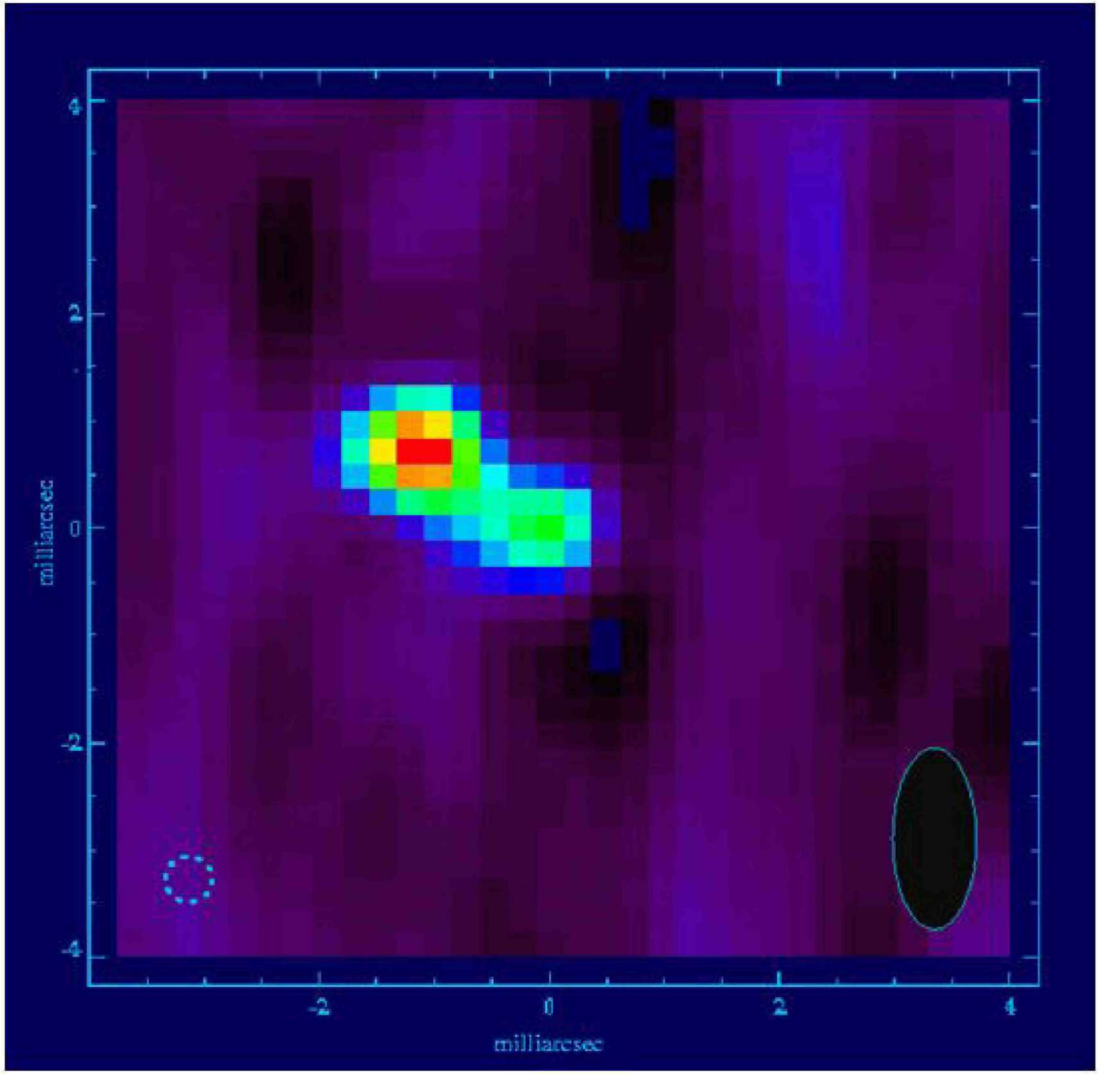
4
2
0
-2
-4
milliarcsec
-2
0
2
4
milliarcsec

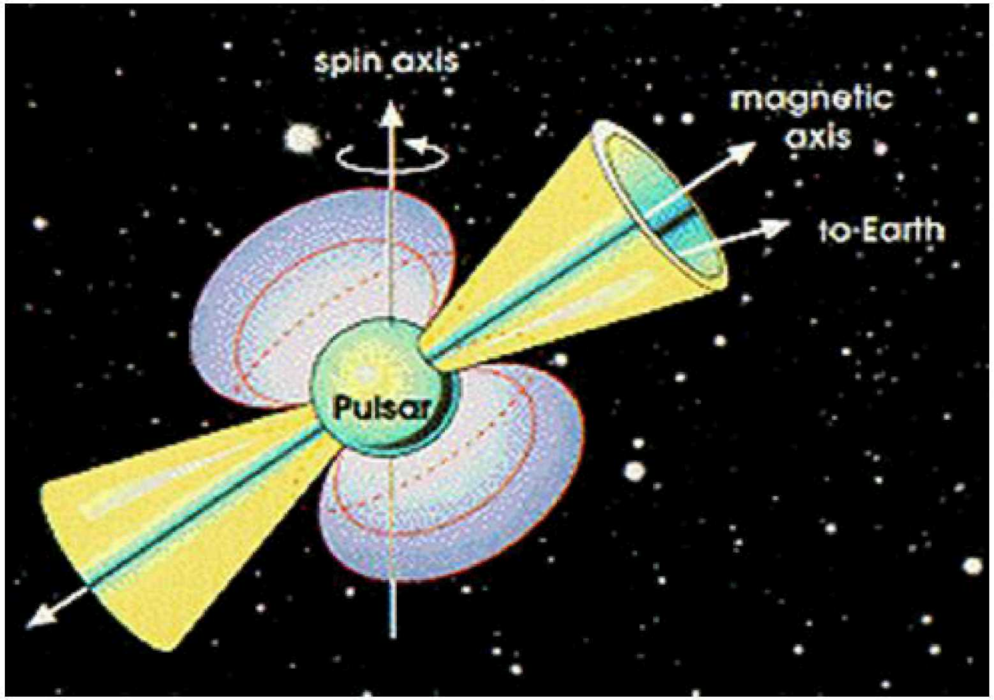
spin axis
magnetic axis
to-Earth
Pulsar

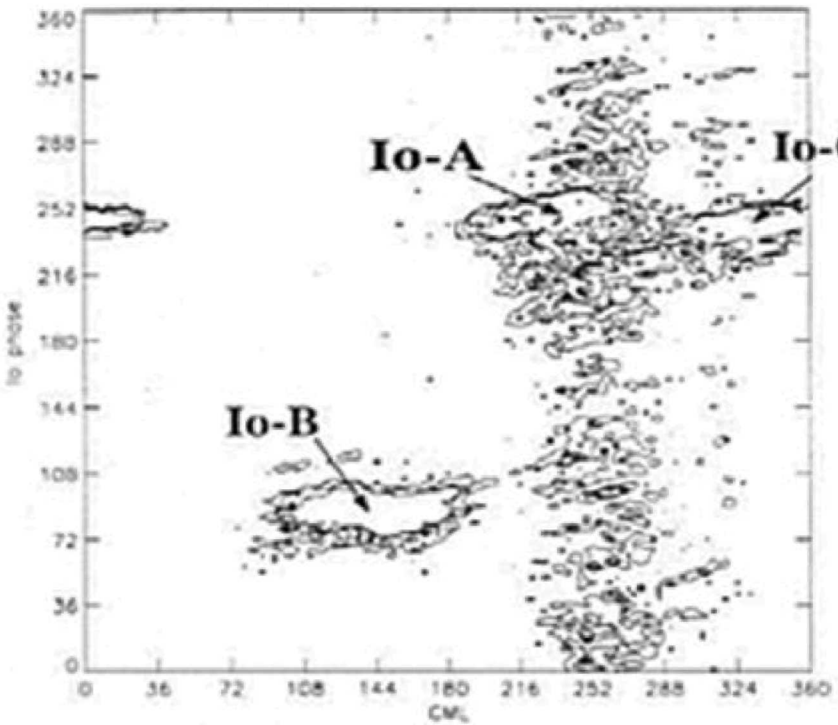
Io-A
Io-C
Io-B
Io phase
CML
0
36
72
108
144
180
216
252
288
324
360

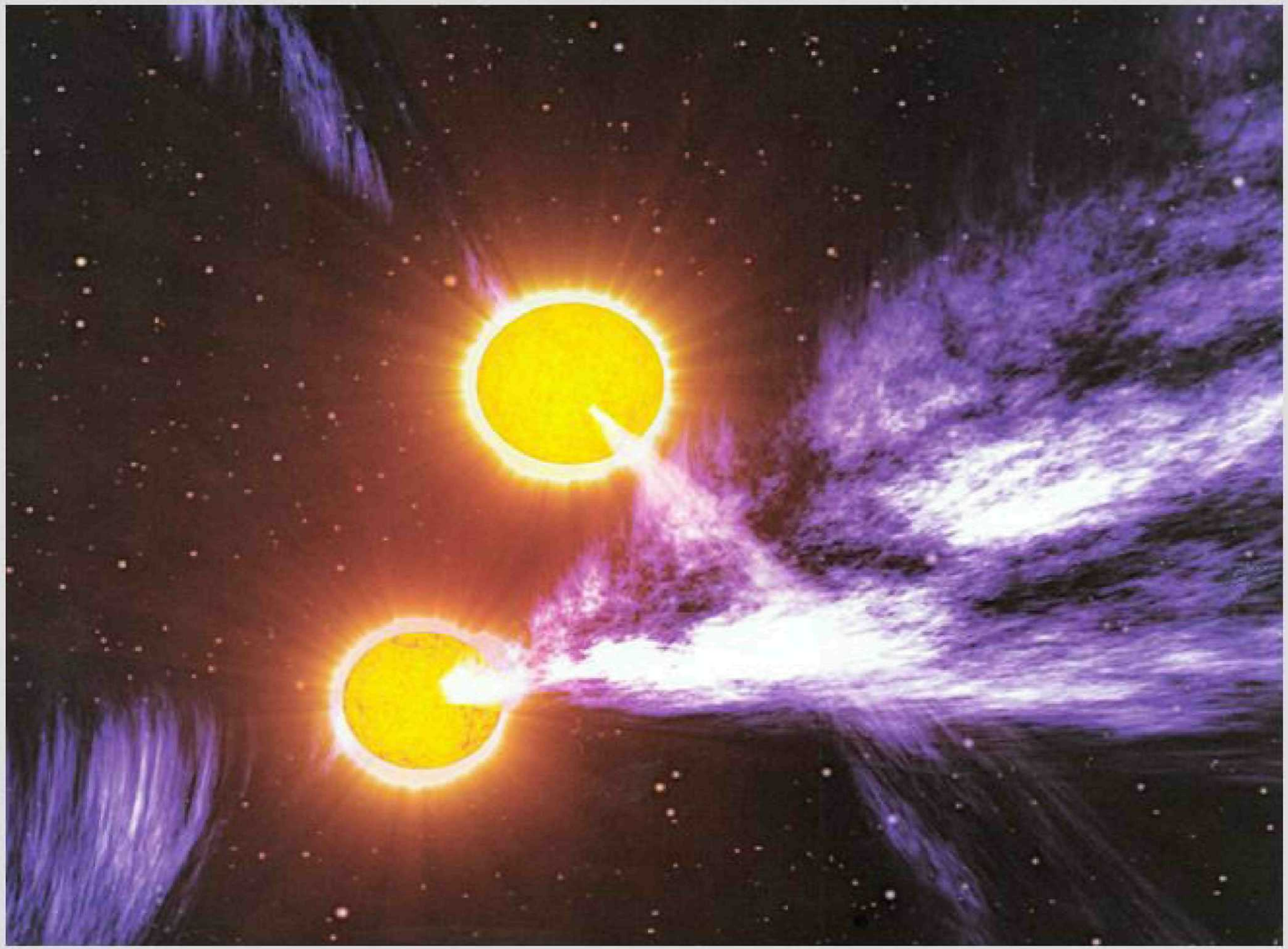

Pulsar Beam

Pulsar model – from observations

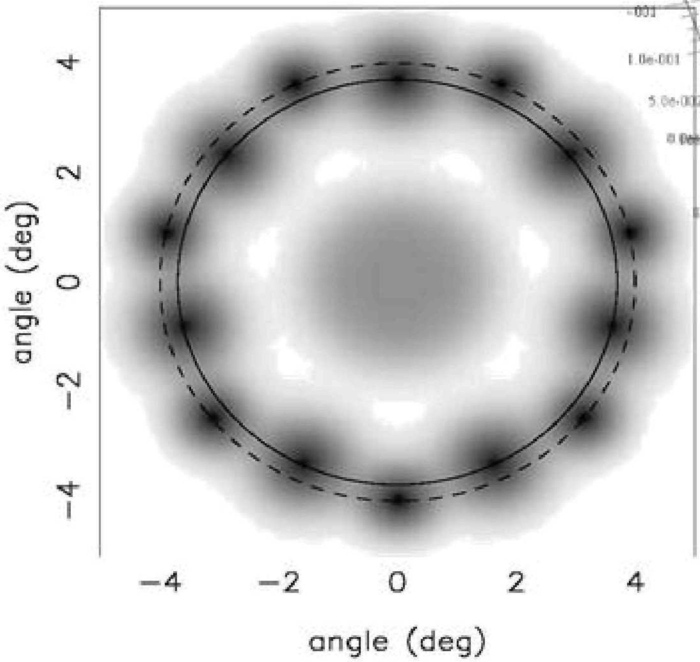

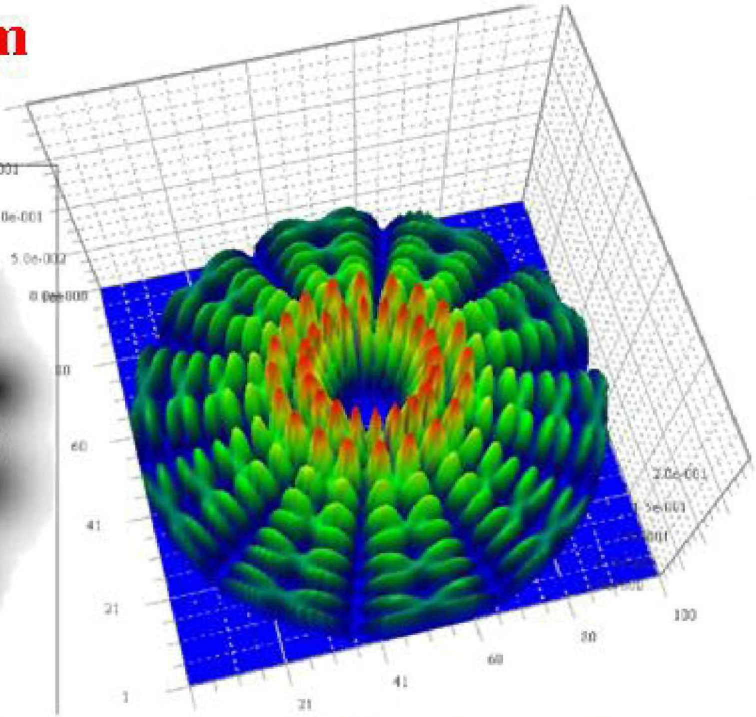

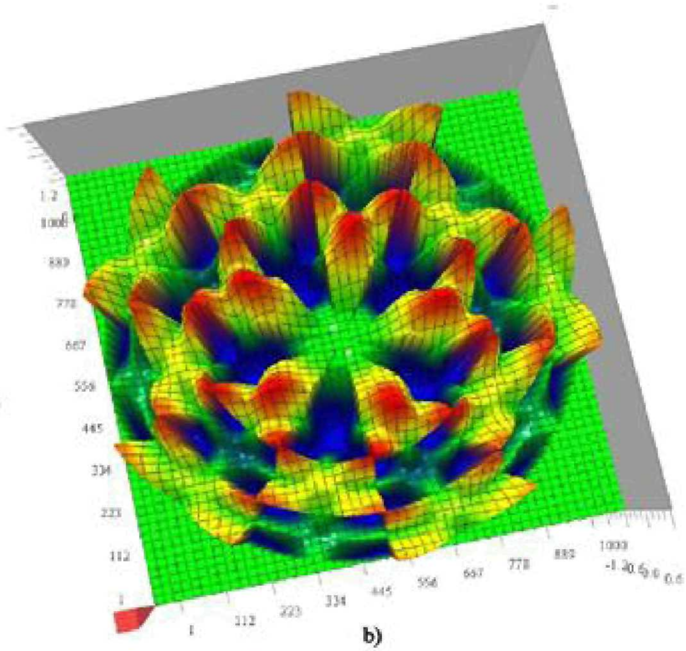

Electron "bunching" – Theory

The black-and-white image on the left is a picture derived from radio observations of many different pulsar "polar caps".

The colour images are simulations of electron "self-organised" bunching in a converging/diverging magnetic geometry …

Laboratory Experiment

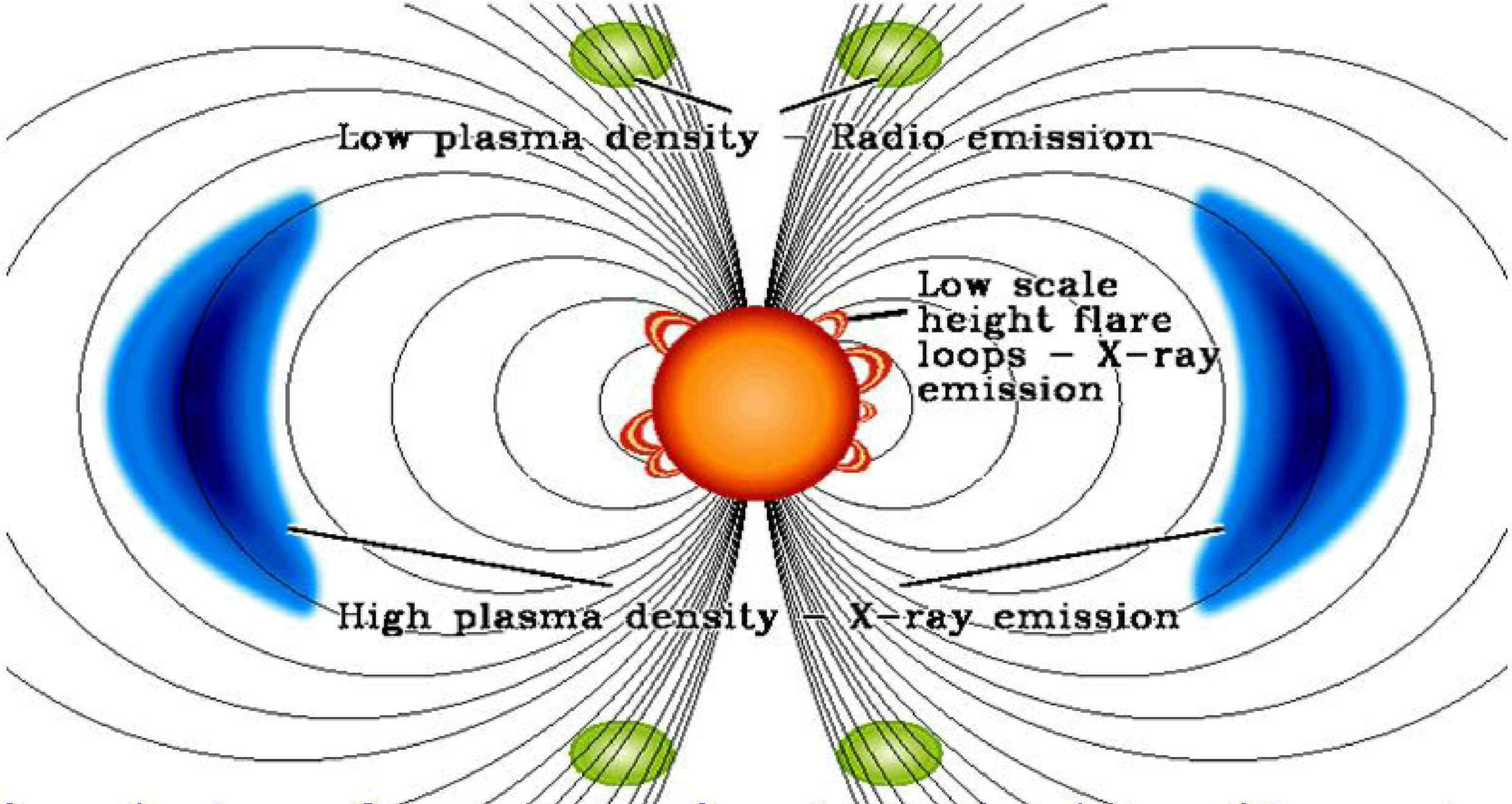

- So, in order to perform an experiment, we simply need to construct a converging magnetic field …
- … and then fire in an electron beam!
- (couldn’t be simpler – at least for an astronomer! – it *might* be a little more difficult to actually build …)

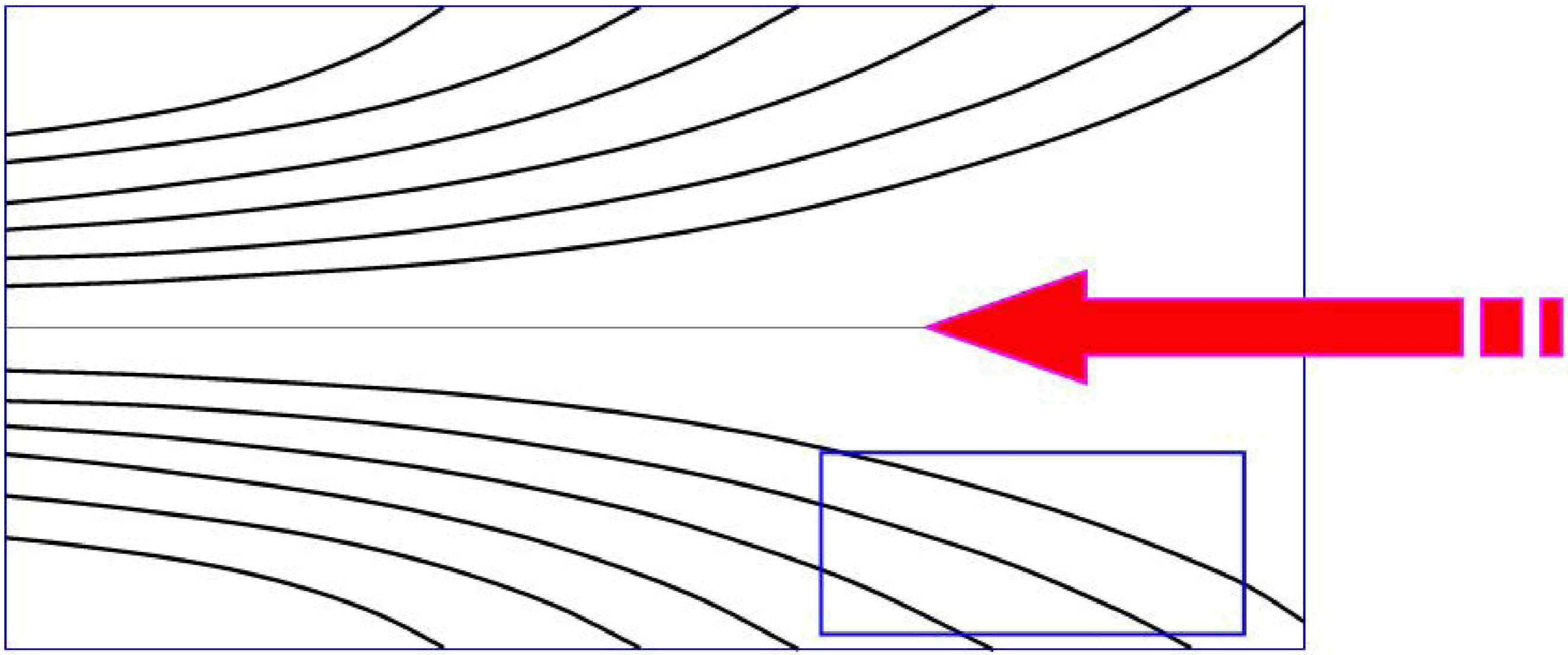

Modelling the Laboratory Experiment

- Shown are some simulations for the laboratory experimental configuration.

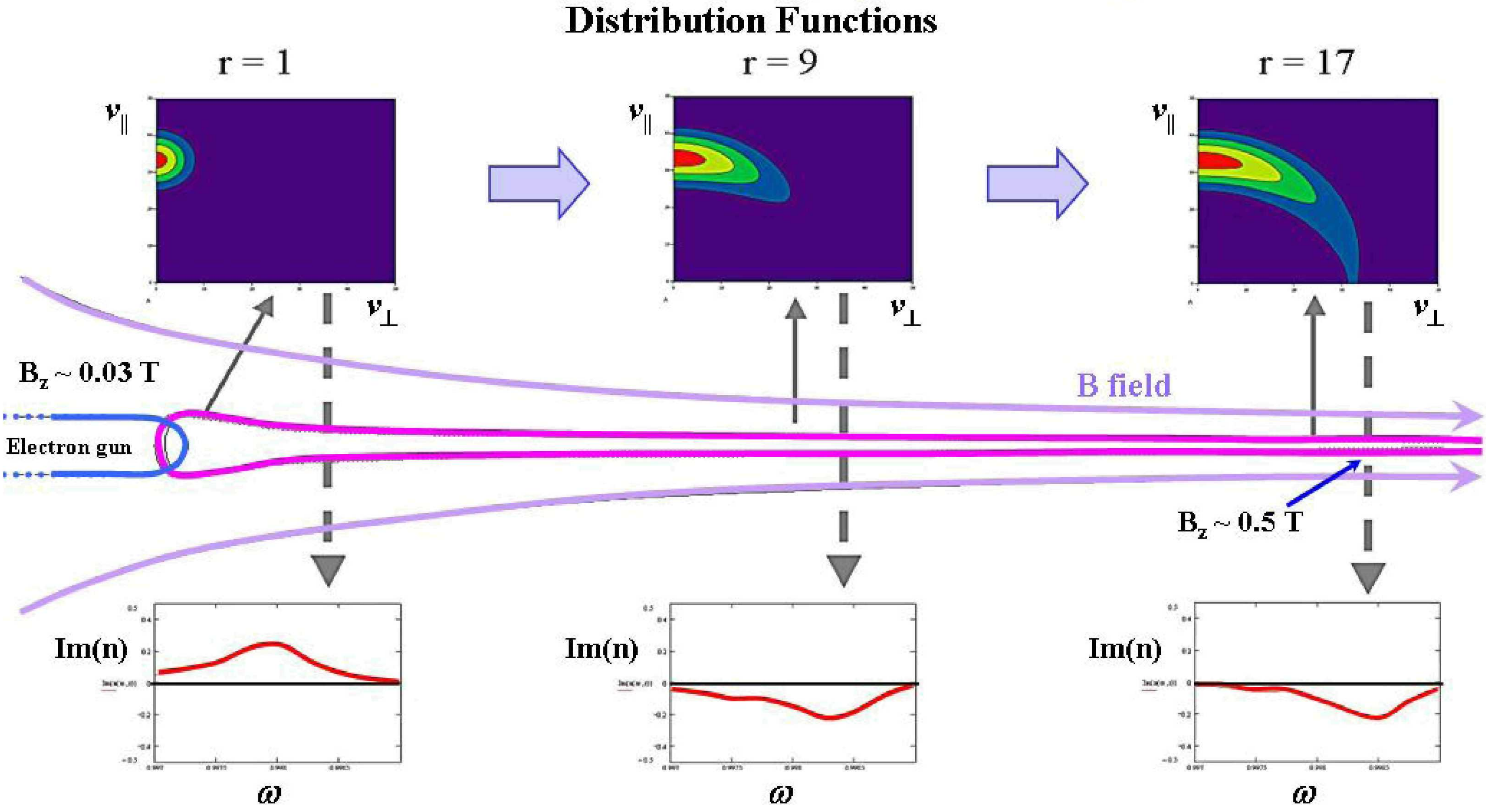

CCLRC Rutherford Appleton Laboratory

PiC Simulations

- The experiment was developed with the support of simulations using the PiC code KARAT
- It was impossible to achieve large magnetic compressions (~30) within the confines of the laboratory environment whilst retaining adiabatic conditions, the simulations codes were used to model a realistic compression regime
- A 2D cylindrically symmetric system was chosen for the simulation model, the simulation was tuned to bring the electrons into resonance with azimuthally symmetric modes of radiation
- Radiation emissions from the electrons were modelled, including the impact on their distribution functions

CCLRC Rutherford Appleton Laboratory

Electron Beam Trajectories Predicted by KARAT

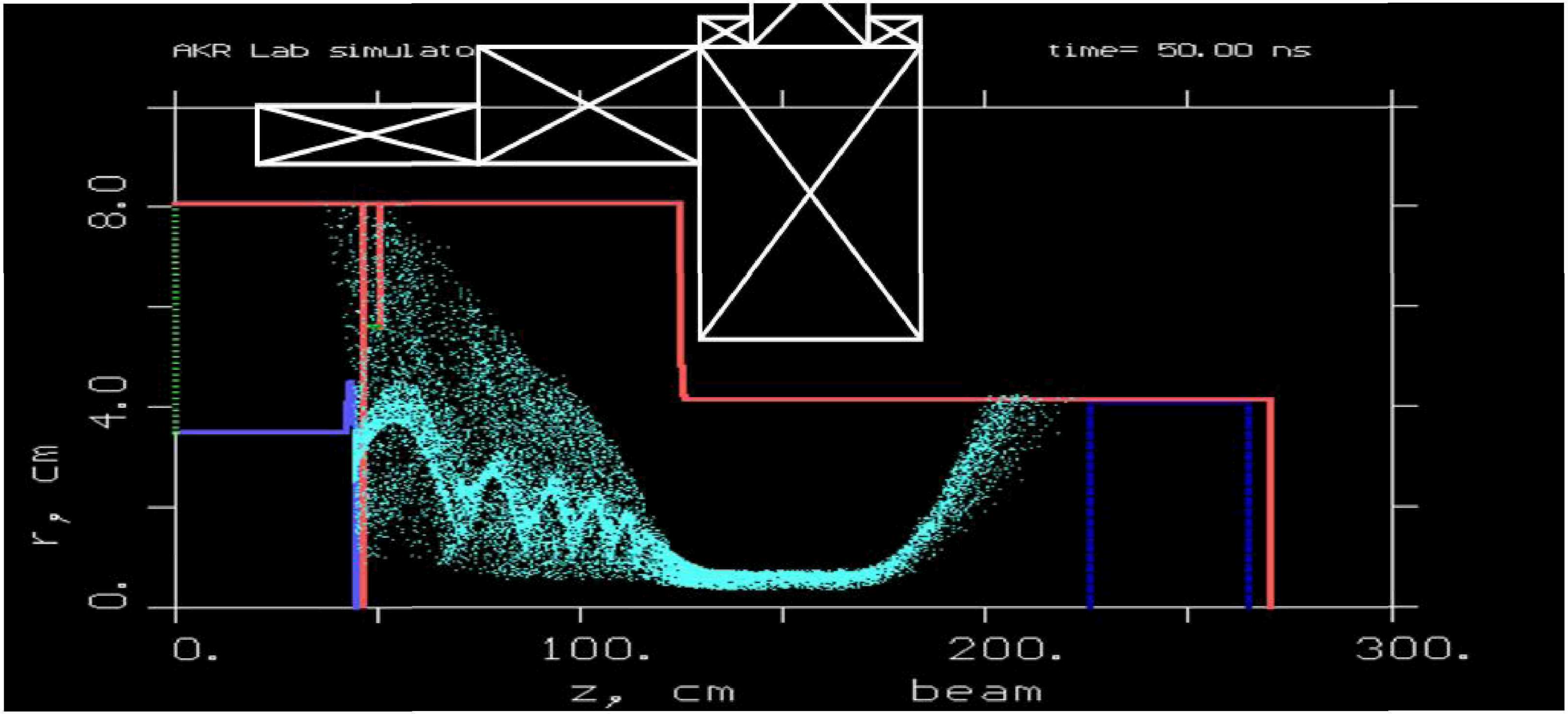

Electron beam trajectory and simulation geometry with solenoids depicted for reference

CCLRC
Rutherford Appleton Laboratory

Beam distribution results from the KARAT simulation code.

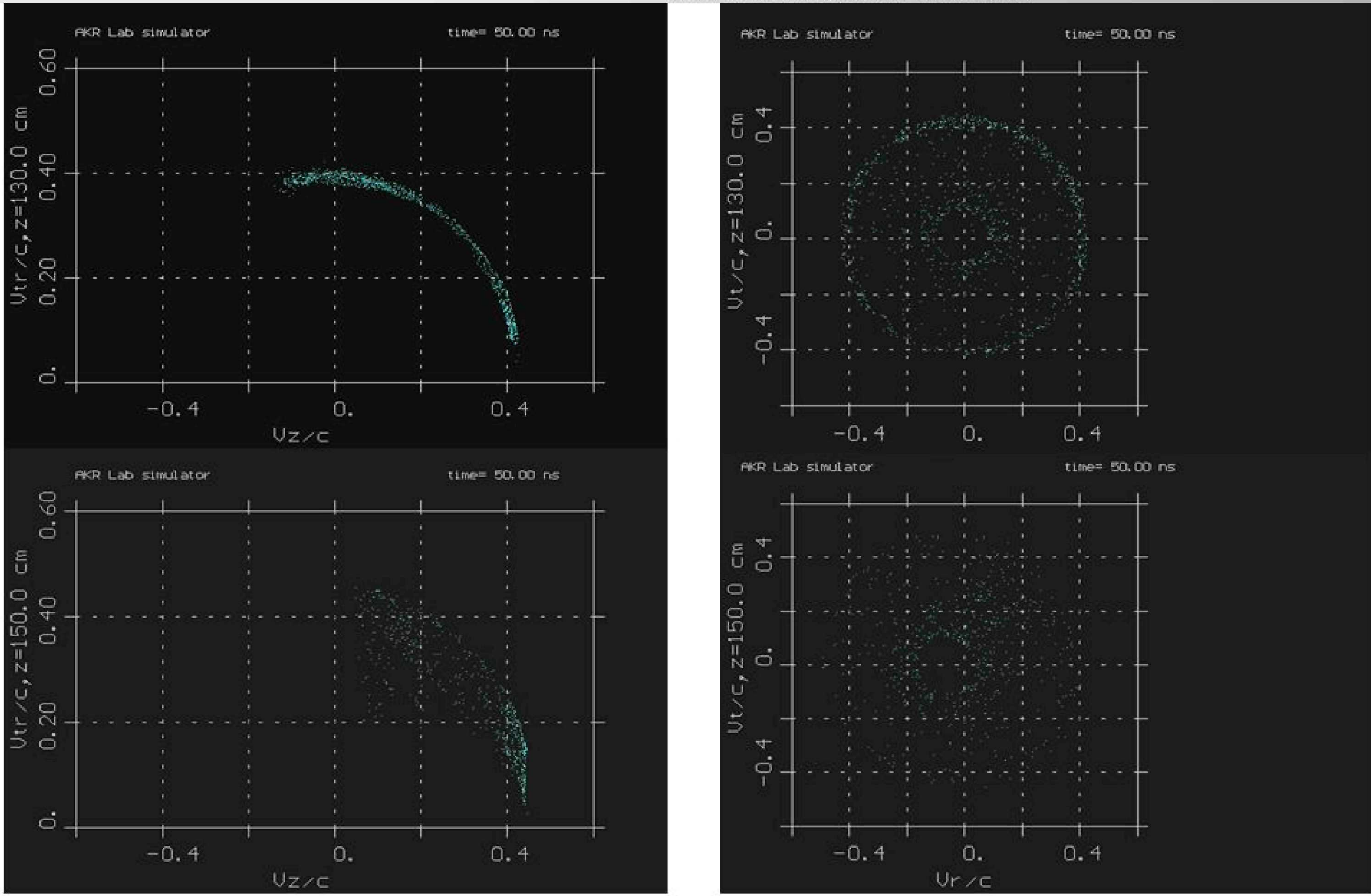

Microwave Output Predictions

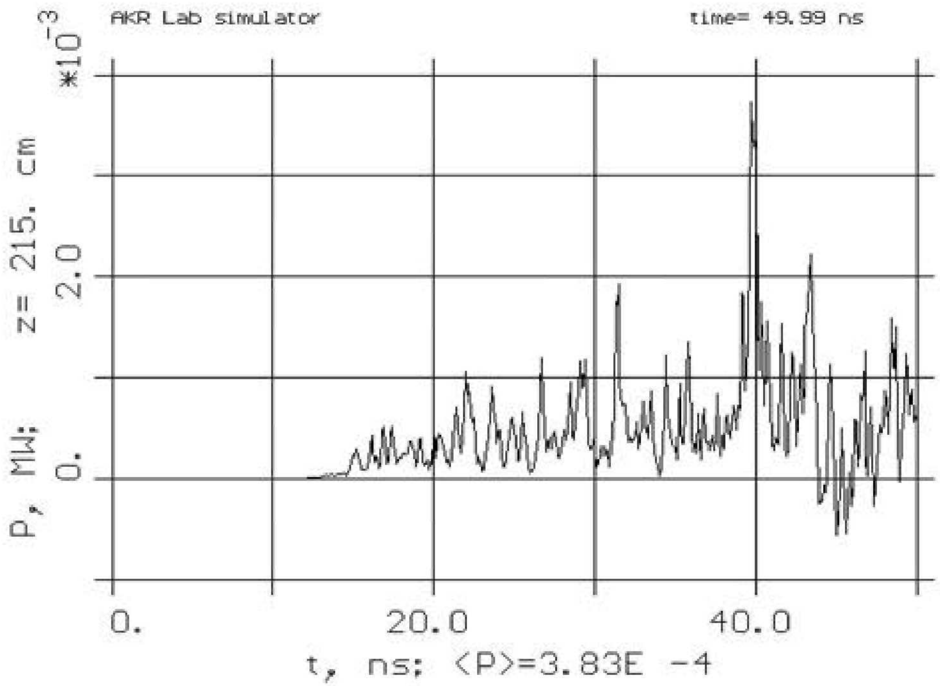

~11.6-11.7 GHz!

NB: Note predicted frequency

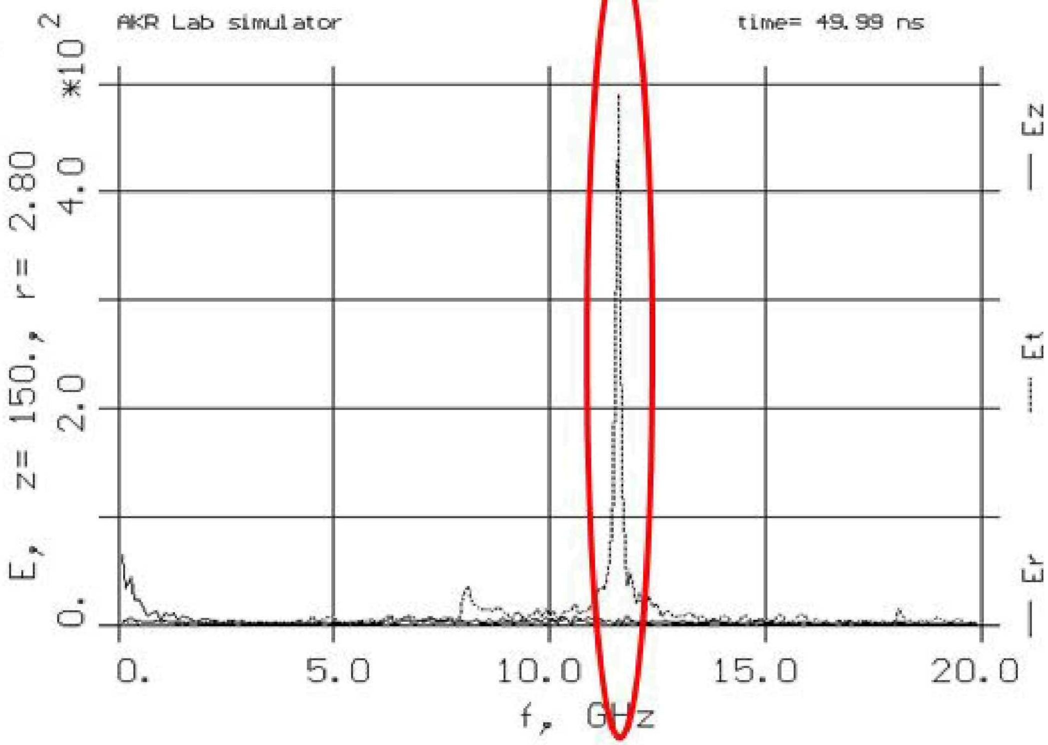

Solenoids

- Construct from 7mm OD, 2mm ID insulated OFHC copper tubing (total length > 1km) wound on non-magnetic formers, tubing is core cooled by water at 20Bar
- Drive up to 6 Solenoids independently up to 600A with 120kW DC power supplies
- Allows flexible control of the magnetic field configuration and therefore of the rate and degree of magnetic compression

Solenoid Configuration

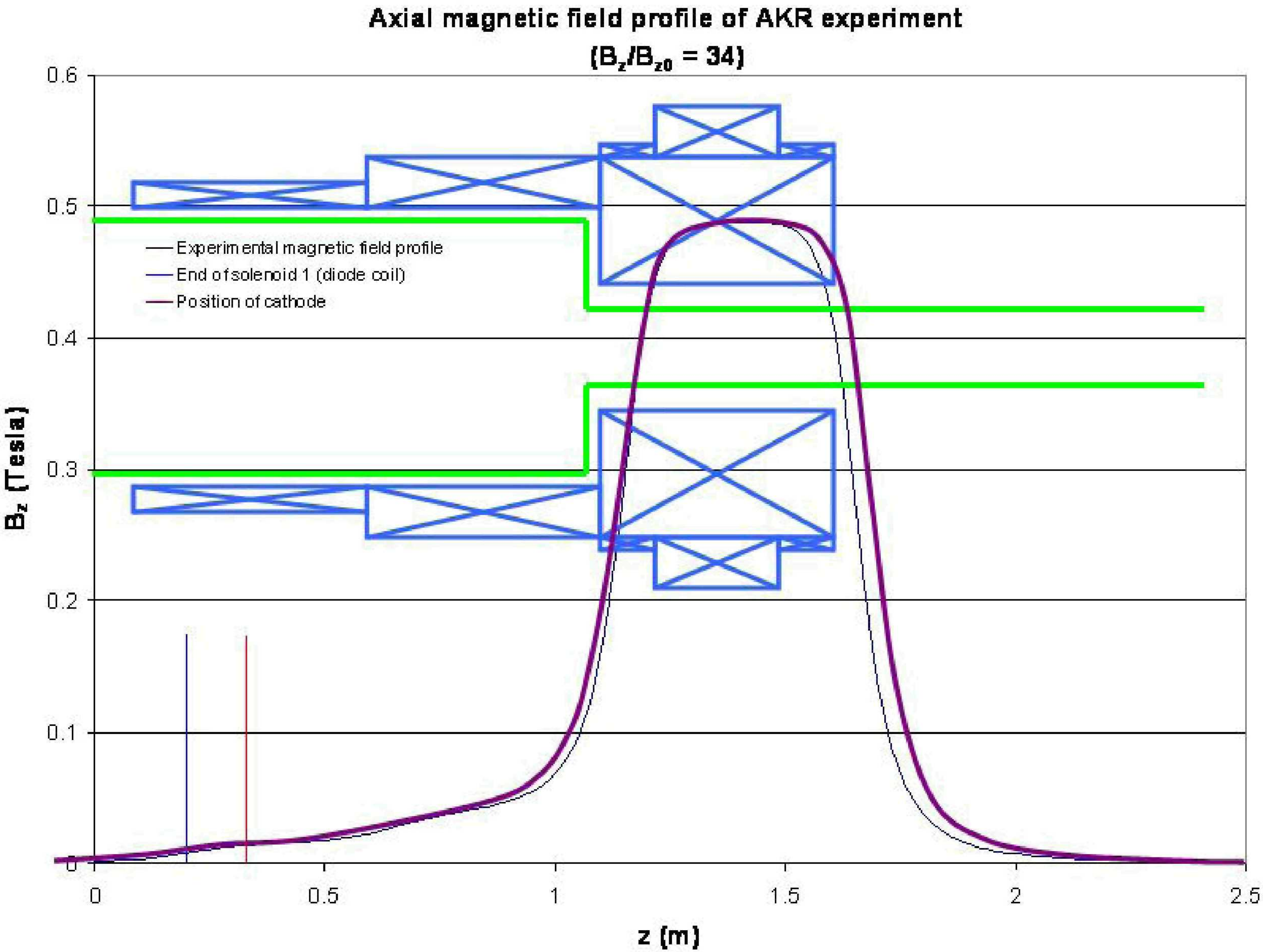

During Construction …

Solenoid 1: 4 Layers, Length = 0.25m, R_i = 0.105m, Current = 75A.
Solenoid 2: 2 Layers, Length = 0.5m, R_i = 0.105m, Current = 60A.
Solenoid 3: 10 Layers, Length = 0.5m, R_i = 0.05m, Current = 250A.
Solenoid 4: 2 Layers, Length = 0.11m, R_i = 0.12m, Current = 250A.
Solenoid 5: 2 Layers, Length = 0.11m, R_i = 0.12m, Current = 250A.

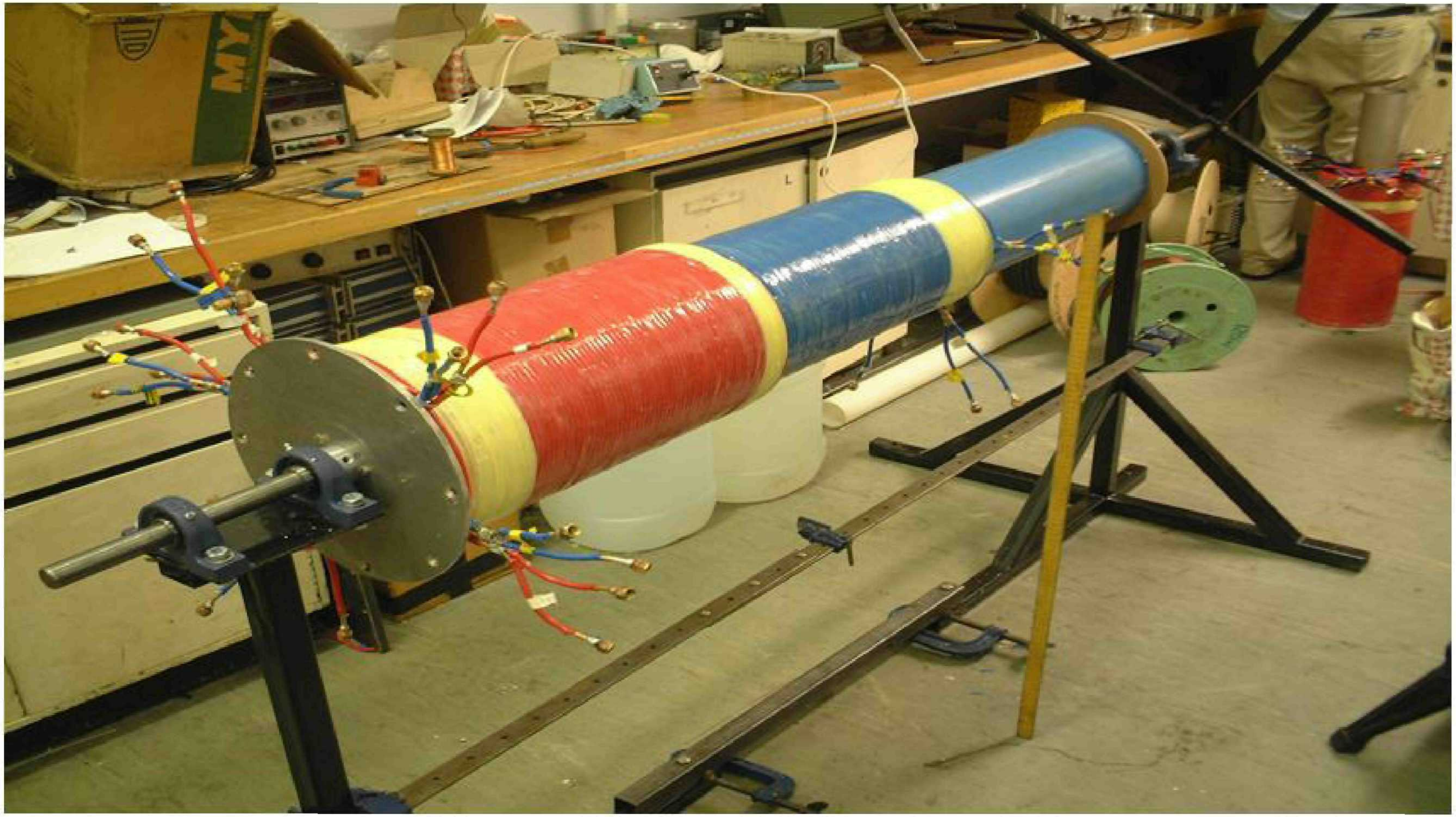

Solenoids 1 and 2 complete and mounted on the solenoid winding rig. A shared UPVC former was used with the excess visible next to the end capstan.

CCLRC Rutherford Appleton Laboratory

Experimental Progress

- Coil fabrication complete, experimental chamber evacuated to 10^{-9} Bar
- Water cooling pump/distributors and drive power supplies installed
- Major apparatus assembly completed
- Experiments now underway

CCLRC
Rutherford Appleton Laboratory

Apparatus

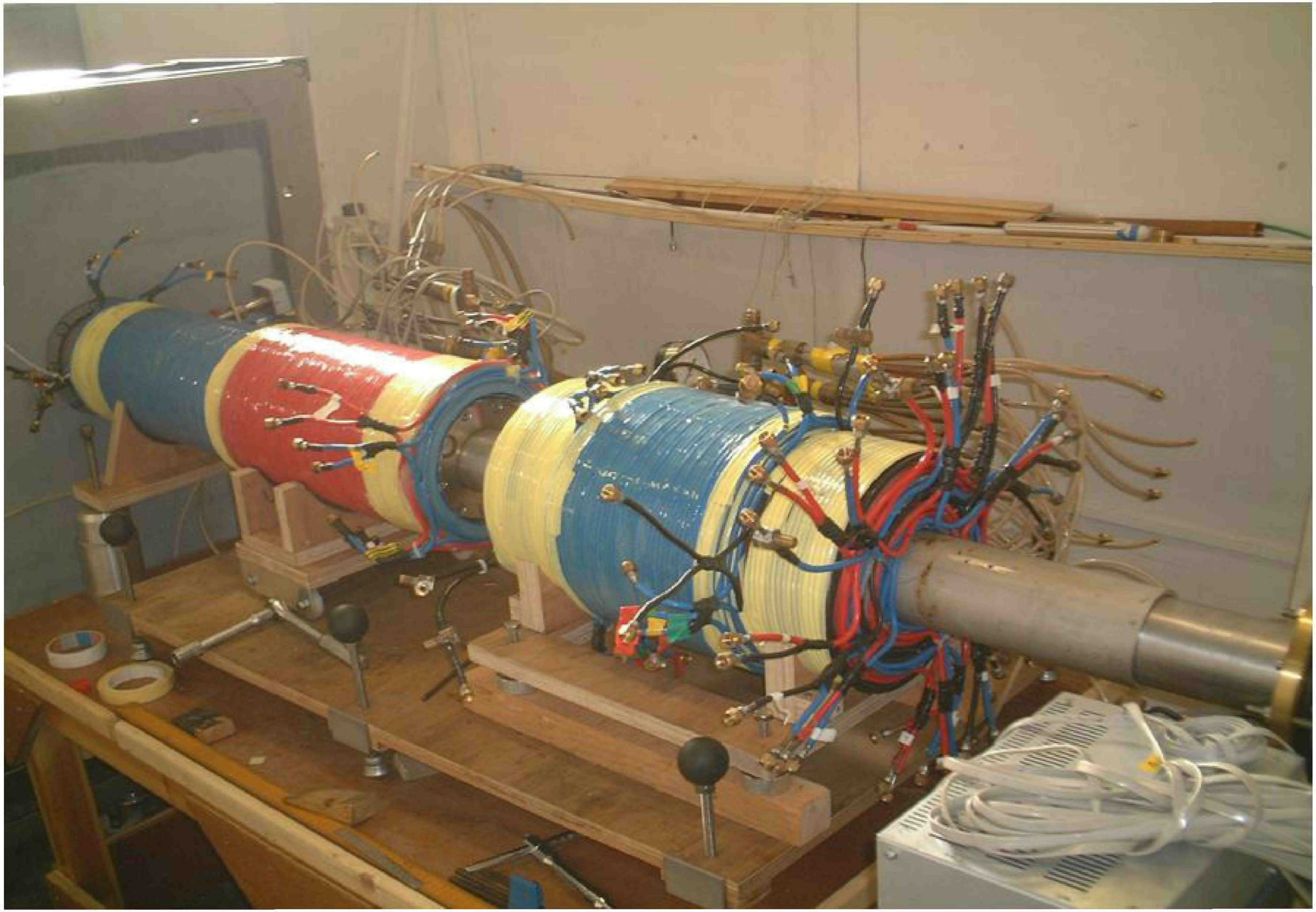

Electron Gun and Faraday Cup

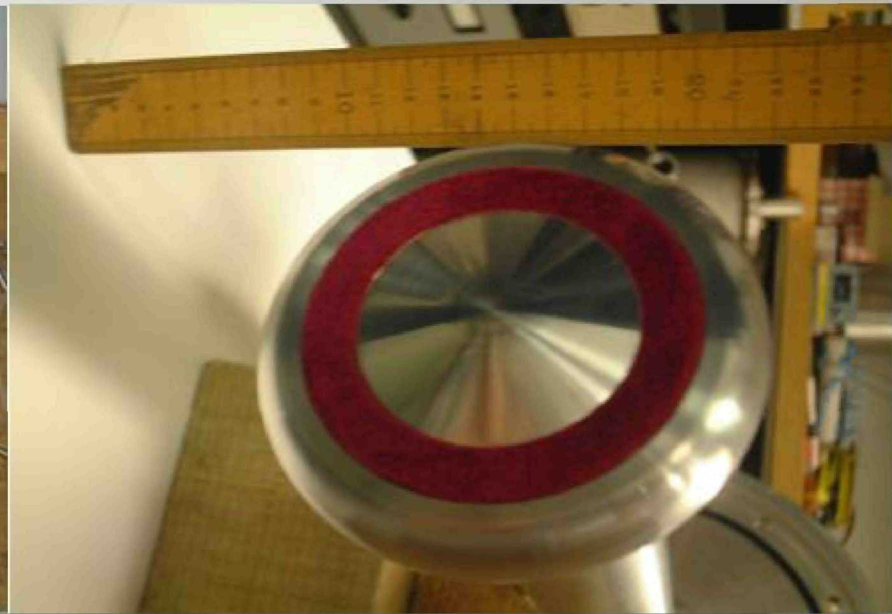

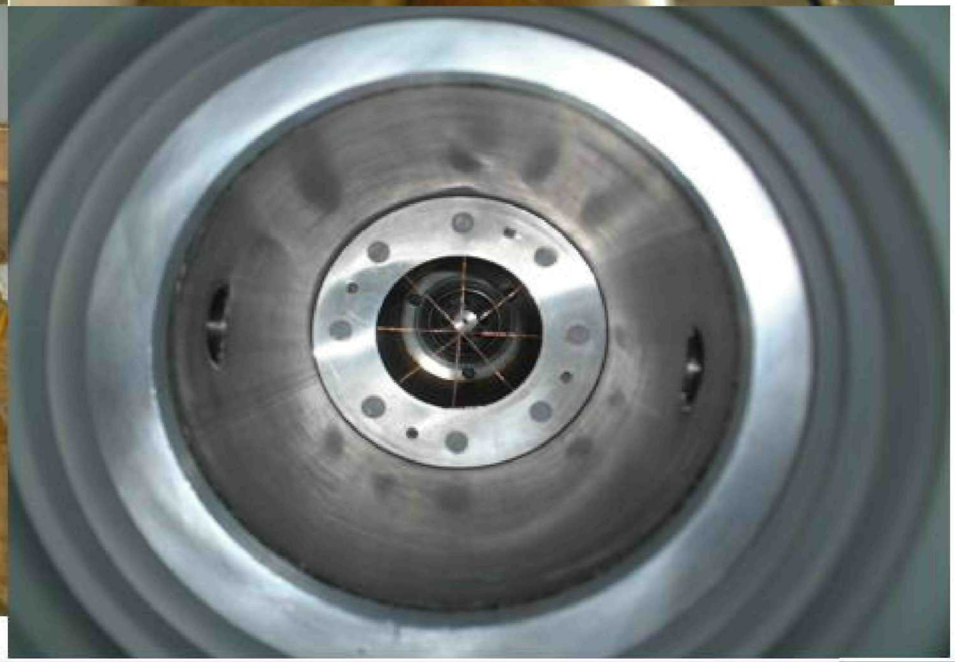

Microwave output frequency

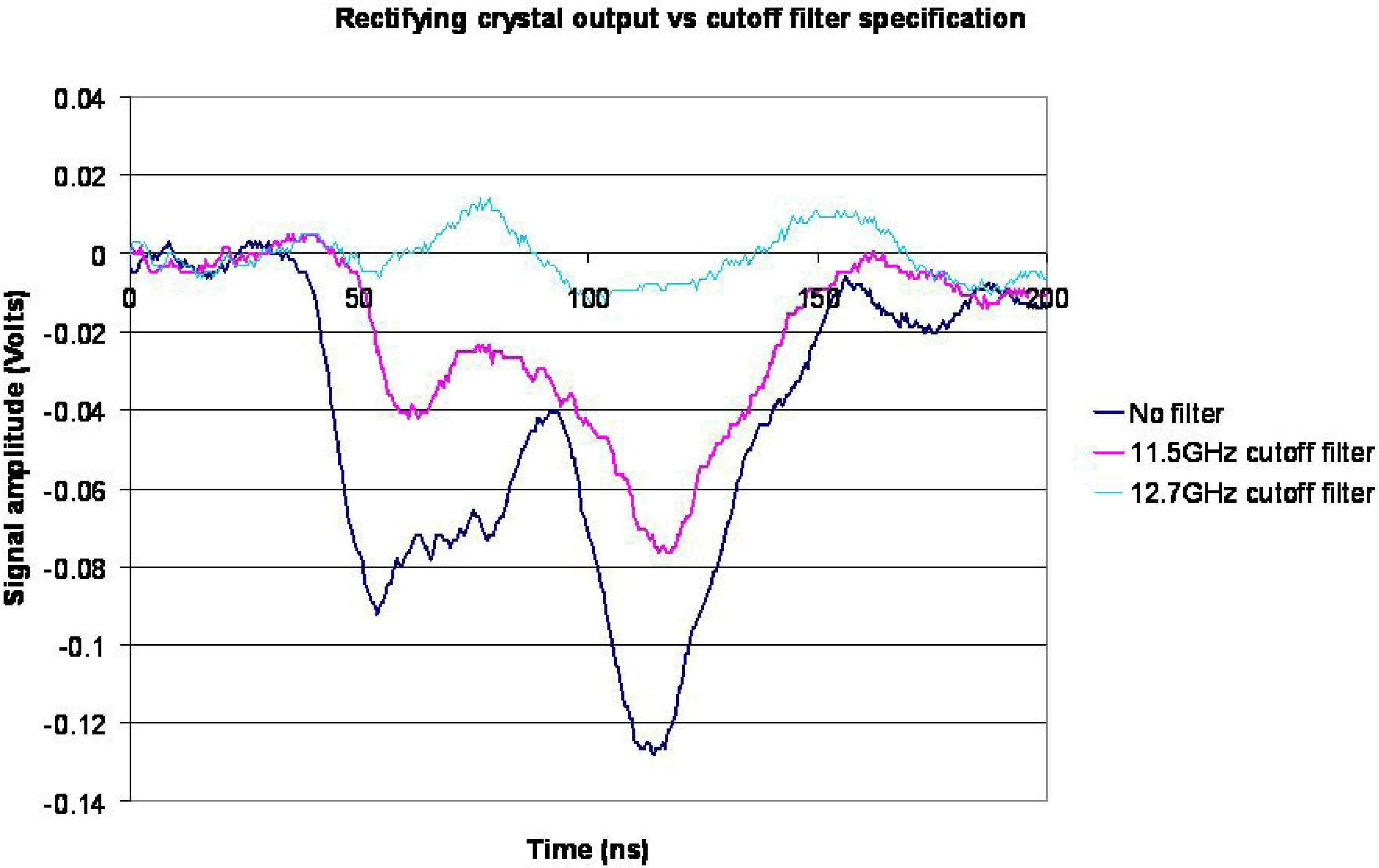

Microwave output frequency

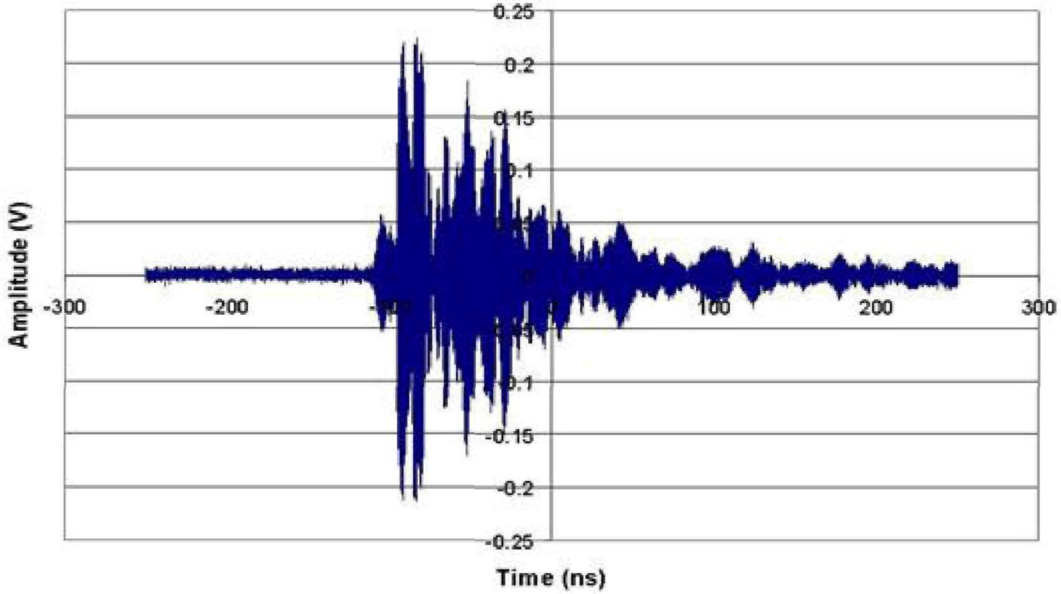

NB: Note *observed* frequency ~11.6-11.7 GHz!

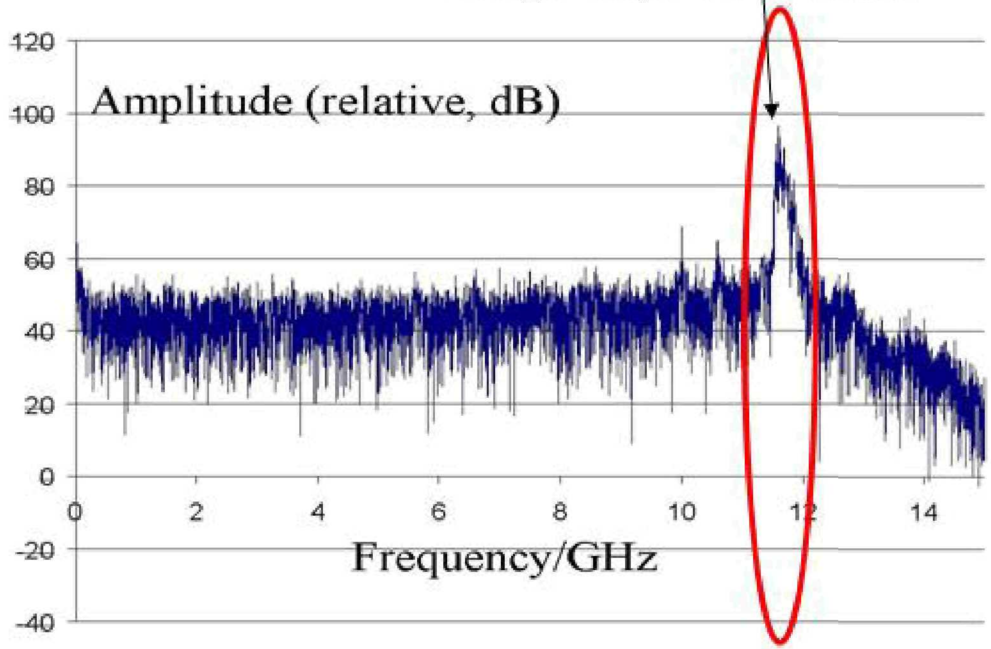

Microwave Antenna Pattern

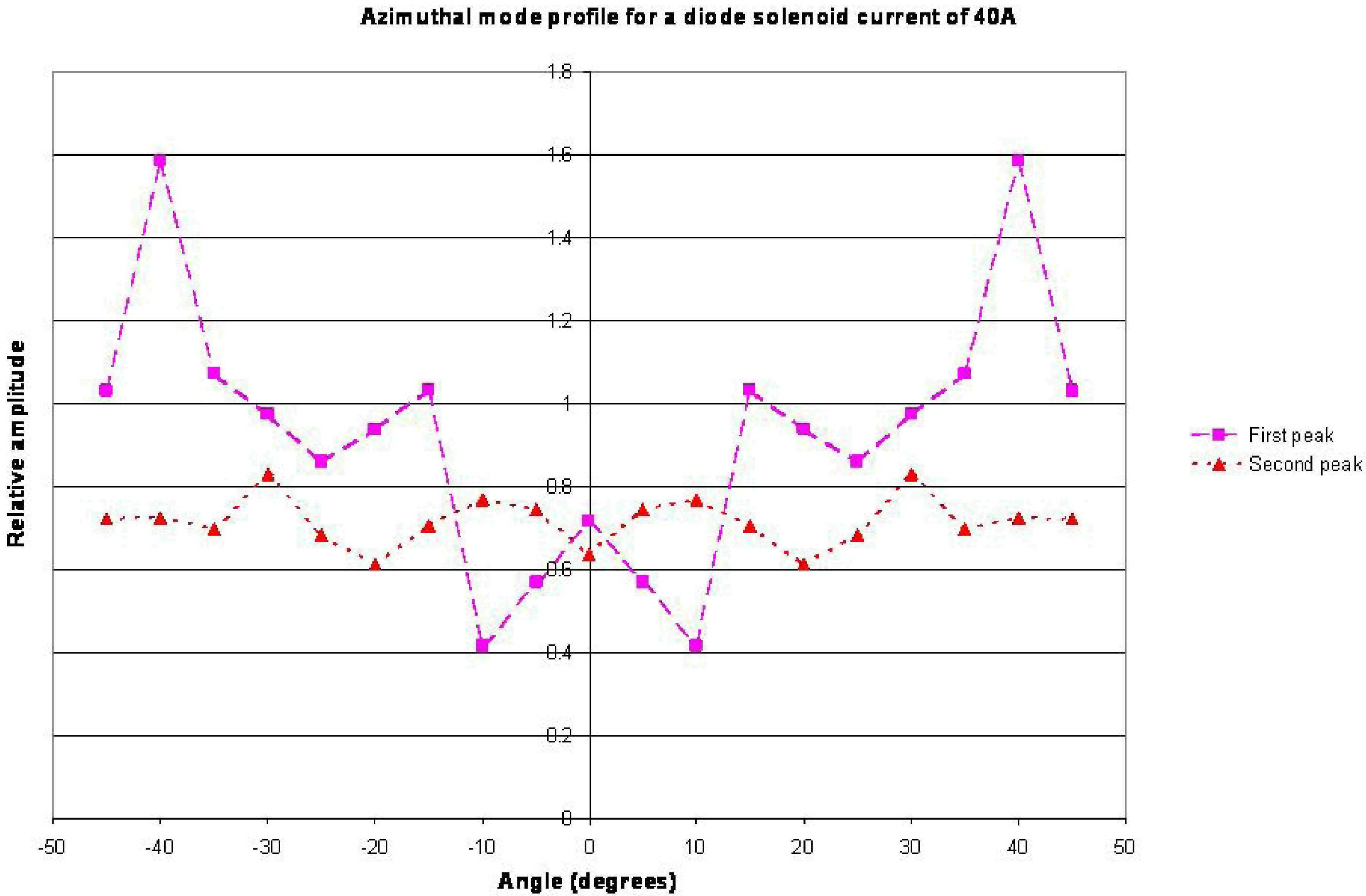

CCLRC Rutherford Appleton Laboratory

Mirroring of Electron Beam

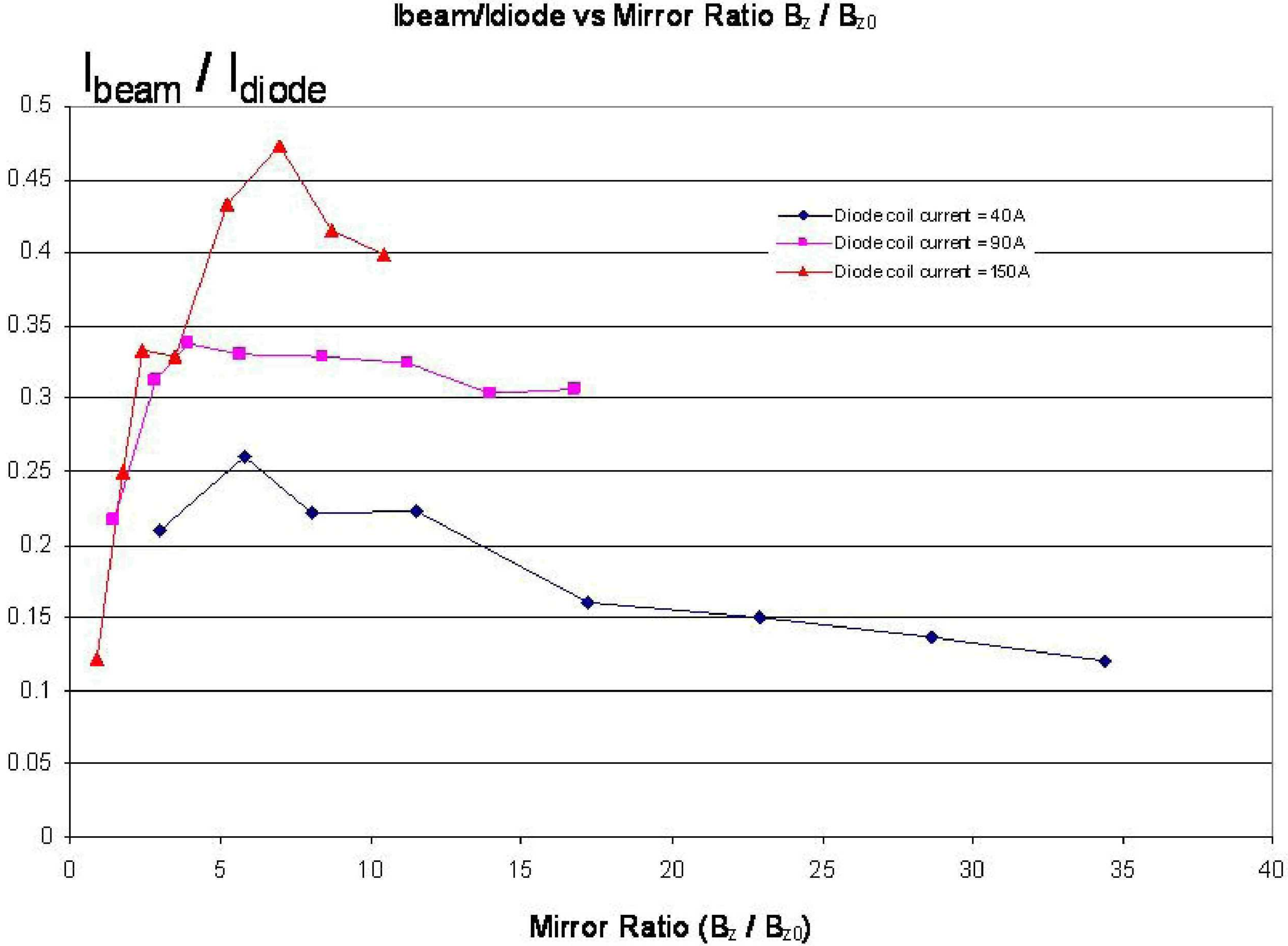

CCLRC Rutherford Appleton Laboratory

Summary

- An experiment has been devised to investigate a proposed new mechanism for Auroral Kilometric Emission
- The apparatus has been developed in conjunction with PiC code simulations of the geometry and field configurations to allow the formation of an electron beam having a horseshoe distribution in phase space via a highly configurable process of magnetic compression
- Major component fabrication is now complete
- Experiments to test the validity of the mechanism are underway with the results being compared against recent developments of the theory (at St. Andrews University) to account for a metallic bounded geometry

Conclusions

- The cyclotron maser instability generated by the horseshoe distributions observed in the auroral zone can easily account for the AKR emission, stellar radio emission, pulsars?.
- Laboratory AKR Experiment – "table-top aurora"
- Confirms horseshoe generation mechanism
- Bandwidth and mode conversion agree with theory
- We have direct access to a "laboratory" for studying the radio emission from planetary and stellar sources!

CCLRC
Rutherford Appleton Laboratory

Future Work

- Accurate characterisation of the emitted radiation (frequency, power modal content)
- Investigate growth rate of the instability by reconfiguring the apparatus to act as an amplifier
- Compare measurements of growth rate with theory
- Understand if the instability may have practical implementations

Acknowledgements

This work was funded by the EPSRC (new extension grant applied for!)